The 1982 revised criteria for the classification of systemic lupus erythematosus, Arthritis Rheum. 25 (1982) 1271–1277.
[22] M.C. Hochberg, Updating the American College of Rheumatology revised criteria for the classification of systemic lupus erythematosus, Arthritis Rheum. 40 (1997) 1725.
[23] O. Ferrigno, T. Virolle, Z. Djabari, J.P. Ortonne, R.J. White, D. Aberdam, Transposable B2 SINE elements can provide mobile RNA polymerase II promoters, Nat. Genet. 28 (2001) 77–81.
[24] S.T. Smale, D. Baltimore, The "initiator" as a transcription control element, Cell 57 (1989) 103–113.
[25] K.L. Moser, B.R. Neas, J.E. Salmon, H. Yu, C. Gray-McGuire, N. Asundi, G.R. Bruner, J. Fox, J. Kelly, S. Henshall, D. Bacino, M. Dietz, R. Hogue, G. Koelsch, L. Nightingale, T. Shaver, N.I. Abdou, D.A. Albert, C. Carson, M. Petri, E.L. Treadwell, J.A. James, J.B. Harley, Genome scan of human systemic lupus erythematosus: evidence for linkage on chromosome 1q in African-American pedigrees, Proc. Natl. Acad. Sci. USA 95 (1998) 14869–14874.
[26] P.M. Gaffney, W.A. Ortmann, S.A. Selby, K.B. Shark, T.C. Ockenden, K.E. Rohlf, N.L. Walgrave, W.P. Boyum, M.L. Malmgren, M.E. Miller, G.M. Kearns, R.P. Messner, R.A. King, S.S. Rich, T.W. Behrens, Genome screening in human systemic lupus erythematosus: results from a second Minnesota cohort and combined analyses of 187 sib-pair families, Am. J. Hum. Genet. 66 (2000) 547–556.
[27] J.Y. Chan, M.C. Cheung, P. Moi, K. Chan, Y.W. Kan, Chromosomal localization of the human NF-E2 family of bZIP transcription factors by fluorescence in situ hybridization, Hum. Genet. 95 (1995) 265–269.
[28] K. Itoh, M. Mochizuki, Y. Ishi, T. Ishii, T. Shibata, Y. Kawamoto, V. Kelly, K. Sekizawa, K. Uchida, M. Yamamoto, Transcription factor Nrf2 regulates inflammation by mediating the effect of 15-deoxy-$\Delta^{12,14}$-prostaglandin J_2, Mol. Cell. Biol. 24 (2004) 36–45.
[29] P. Gong, D. Stewart, B. Hu, N. Li, J. Cook, A. Nel, J. Alam, Activation of the mouse heme oxygenase-1 gene by 15-deoxy-$\Delta^{12,14}$-prostaglandin J_2 is mediated by the stress response elements and transcription factor Nrf2, Antioxid. Redox. Signal. 4 (2002) 249–257.

[CANCER RESEARCH 64, 6424–6431, September 15, 2004]

Nrf2 Is Essential for the Chemopreventive Efficacy of Oltipraz against Urinary Bladder Carcinogenesis

Katsuyuki Iida,[1,2] Ken Itoh,[2] Yoshito Kumagai,[3] Ryoichi Oyasu,[4] Kazunori Hattori,[1] Koji Kawai,[1] Toru Shimazui,[1] Hideyuki Akaza,[1] and Masayuki Yamamoto[2]

[1]Department of Urology, Institute of Clinical Medicine, [2]JST-ERATO Environmental Response Project, Center for TARA and Institute for Basic Medical Sciences, and [3]Institute of Community Medicine, University of Tsukuba, Tsukuba, Ibaraki, Japan; and [4]Department of Pathology, Northwestern University Feinberg School of Medicine, Chicago, Illinois

ABSTRACT

The induction of phase 2 detoxifying enzymes, such as UDP-glucuronosyltransferases (UGTs), in response to an array of naturally occurring and synthetic agents, such as oltipraz (4-methyl-5-[2-pyrazinyl]-1,2-dithiole-3-thione), provides an effective means of protection against a variety of carcinogens. Transcription factor Nrf2 is an essential regulator of the inducible expression of detoxifying enzyme genes by chemopreventive agents. In this study, we investigated in Nrf2-deficient mice the susceptibility to the urinary bladder-specific carcinogen *N*-nitrosobutyl(4-hydroxybutyl)amine (BBN) and the chemopreventive efficacy of oltipraz. The incidence of urinary bladder carcinoma by BBN was significantly higher in *Nrf2*$^{-/-}$ mice than in wild-type mice; invasive carcinoma was found in 24.0 and 38.5% of wild-type and *Nrf2*$^{-/-}$ mice, respectively. Oltipraz induced the phase 2 enzymes responsible for BBN detoxification in the liver and urinary bladder in an Nrf2-dependent manner. As expected, therefore, oltipraz decreased the incidence of urinary bladder carcinoma by BBN in wild-type mice but had little effect in *Nrf2*$^{-/-}$ mice. In wild-type mouse liver, oltipraz significantly induced BBN glucuronidation and decreased the urinary concentration of *N*-nitrosobutyl(3-carboxypropyl)amine, a proximate carcinogen of BBN. Importantly, BBN was found to suppress the expression of *UGT1A* specifically in the urinary bladder. This suppression was counteracted by oltipraz in wild-type mice but not in *Nrf2*$^{-/-}$ mice. These results show that Nrf2 and its downstream target genes are responsible for BBN detoxification. Furthermore, oltipraz prevents carcinogenesis by BBN by enhancing detoxification of this carcinogen in the liver and urinary bladder.

INTRODUCTION

The relationship between chemical exposure and urothelial cancer has been well established since 1895, when it was suggested that men working in the dye industry were at increased risk of bladder cancer (1). 2-Naphthylamine subsequently was determined to be one of the causative agents (2). Currently, cigarette smoking is considered a major risk factor for the development of bladder cancer in industrialized countries (1). Similarly, *N*-nitroso compounds (NOCs) have been proposed as etiologic agents of bladder cancer associated with schistosomiasis (3). NOCs also are thought to play roles in the carcinogenesis of the stomach, esophagus, and pharynx in humans (4). *N*-nitrosodibutylamine, which was first identified as a rat bladder carcinogen, has been detected as a pollutant in tobacco smoke, corrosion inhibitor, food, and rubber products (5). Although it exists in a low concentration, it is considered practically as carcinogenic to humans (6). *N*-nitrosodibutylamine is metabolized mainly in the liver, and tumor induction in the rat bladder seems to depend on the formation of two ω-oxidized metabolites, *N*-nitrosobutyl(4-hydroxybutyl)amine (BBN) and its proximate carcinogen *N*-nitrosobutyl(3-carboxypropyl)amine (BCPN; ref. 7). Oral administration of BBN to rats and mice induces cancer specifically in the urinary bladder (8). BBN-induced urinary bladder carcinogenesis in rodents is an excellent model system to understand the carcinogenic mechanisms by NOC.

Several lines of epidemiologic and experimental evidence suggest that a decreased expression in carcinogen-detoxifying enzymes, such as *N*-acetyl transferase 2 (9, 10), glutathione *S*-transferase (GST) M1 (9, 11), NAD(P)H quinone oxidoreductase (NQO1; ref. 12), and UDP-glucuronosyltransferase (UGT) 1A (13), is associated with urinary bladder cancer. The urinary bladder-specific carcinogenic effect of BBN may result, at least in part, from the metabolic fate of the compound because BCPN, the major urinary metabolite of BBN, has been shown to have carcinogenic effects on urothelial cells (14, 15). Following α-hydroxylation, BCPN and BBN are chemically cleaved to their corresponding alkylcarbonium ion that binds covalently to DNA and enhances carcinogenesis (16).

Carcinogens are normally detoxified by conjugation with water-soluble cofactors. Typical examples of such cofactors are glutathione and glucuronic acid, which are conjugated to carcinogens through the actions of GSTs and UGTs, respectively. These conjugating enzymes have been categorized as phase 2 detoxifying enzymes (17). It has been proposed that induction of phase 2 detoxifying enzyme genes plays a major role in protection against carcinogens (18). A recognized characteristic action of chemopreventive agents, including the phenolic antioxidants 2,3-butyl-4-hydroxyanisole (19) and 1,2-dithiole-3-thione (20) and the isothiocyanates (21), is their potential to induce phase 2 enzymes. Oltipraz (4-methyl-5-[2-pyrazinyl]-1,2-dithiole-3-thione) represents one of the most potent inducers of phase 2 enzymes (22, 23).

The induction of phase 2 enzyme genes is regulated by their *cis*-acting antioxidant response element (ARE) or electrophile responsive element (EpRE; refs. 24–26). Transcriptional factor Nrf2 binds to and regulates transcription through the ARE/EpRE after heterodimerizing with one of the small Maf proteins (27–29). Germline mutant mice specifically lacking the *Nrf2* gene have been established (30, 31). When we treated these mice with 2,3-butyl-4-hydroxyanisole, we found that *Nrf2*$^{-/-}$ mice lack the inducible expression of phase 2 and antioxidant enzymes, providing conclusive evidence for the notion that Nrf2 regulates their transcription (30).

An obvious hypothesis then is that *Nrf2*$^{-/-}$ mice are more susceptible to oxidative and electrophilic stresses, and this hypothesis has been tested in various contexts (32–40). For example, the forestomach tumor formation caused by benzo(*a*)pyrene is markedly increased in *Nrf2*$^{-/-}$ mice, and the chemoprotective activities of oltipraz and sulforaphane were lost (33–35). Similarly, *Nrf2*$^{-/-}$ mice are more susceptible to the acute toxicities of acetaminophen, diesel exhaust, 2,3-butyl-4-hydroxytoluene, and hyperoxia (36–40). These results argue that the Nrf2-mediated induction of phase 2 and antioxidant enzymes is critical for cellular defense against electrophilic and oxidative stresses. The results further suggest that oltipraz prevents

Received 5/30/04; revised 7/9/04; accepted 7/21/04.

Grant support: JST-ERATO, JSPS, the Ministry of Education, Science, Sports and Technology, the Ministry of Health, Labor and Welfare, the Atherosclerosis Foundation, and the Naito Foundation.

The costs of publication of this article were defrayed in part by the payment of page charges. This article must therefore be hereby marked *advertisement* in accordance with 18 U.S.C. Section 1734 solely to indicate this fact.

Requests for reprints: Masayuki Yamamoto, Center for TARA, University of Tsukuba, 1-1-1 Tennoudai, Tsukuba 305-8577, Japan. Phone: 81-298-53-6158; Fax: 81-298-53-7318; E-mail: masi@tara.tsukuba.ac.jp.

chemical carcinogenesis by inducing Nrf2-regulated cytoprotective enzymes.

The contribution of the Nrf2 regulatory pathway in protection against urinary bladder carcinogenesis requires clarification, even though a large number of studies on chemically induced cancer formation have been reported. Thus, we investigated the susceptibility of *Nrf2*$^{-/-}$ mice to the urinary bladder-specific carcinogen BBN and the preventive efficacy of oltipraz in these mice. In wild-type mice, oltipraz up-regulated the detoxification activity of carcinogens in the liver and consequently decreased the BCPN concentration in the urine. Importantly, oltipraz also induced the expression of phase 2 enzyme genes in the wild-type urinary bladder and counteracted BBN-induced suppression of *UGT1A* gene expression. In *Nrf2*$^{-/-}$ mice, loss of Nrf2 significantly enhanced susceptibility to BBN and largely abolished the chemopreventive efficacy of oltipraz. These results show that the cellular defense enzymes under the regulation of Nrf2 play key roles in preventing urinary bladder carcinogenesis.

MATERIALS AND METHODS

Reagents. BBN was purchased from Tokyo Kasei (Tokyo, Japan). The Chemoprevention Branch of the National Cancer Institute (Bethesda, MD) provided the oltipraz. UDP-glucuronic acid (UDPGA) was purchased from Sigma (St. Louis, MO). Dr. Yukio Mori (The Gifu Pharmaceutical University, Gifu, Japan) provided the BCPN.

Animals. Nrf2-deficient mice of ICR/129SV background have been established at the University of Tsukuba (Tsukuba, Ibaraki, Japan; ref. 30). A colony of ICR/129SV background mice were backcrossed for nine generations with C57BL/6 mice, which were purchased from CLEA Japan (Tokyo, Japan). Mice were housed in stainless steel cages in an animal room maintained at 24 ± 2 °C. Mice were maintained with a 12-hour light/dark cycle and fed a purified AIN-76A diet (Oriental MF; Oriental Yeast Co., Tokyo, Japan) and water *ad libitum*.

BBN-Induced Bladder Carcinogenesis. Oltipraz was fed *ad libitum* at the concentration of 250 mg/kg diet from 1 week before carcinogen administration until termination of the study 18 weeks later. BBN was dissolved in tap water to a concentration of 0.05% and supplied *ad libitum* for 8 weeks with the dark bottles. After the experimental period, mice were analyzed by autopsy. Urinary bladders were removed and inflated with and fixed in 10% buffered formalin. Each bladder then was sectioned sagittally, and each cup-shaped area was cut into four pieces. These eight strips of bladder tissue were serially embedded in one block of paraffin, cut into thin sections, and stained with H&E. Bladder lesions were histologically diagnosed according to the criteria of Oyasu *et al.* (41).

RNA Blot Analysis. Total RNAs from liver and whole urinary bladder were extracted with Isogen (Nippon Gene, Toyama, Japan) according to the manufacturer's instructions. Total RNAs (10 μg) were separated by 1.5% agarose gel electrophoresis containing 2.2 mol/L formaldehyde and transferred to nylon membrane. DNA probes for Nrf2 and UGT1A6 have been described previously (37), and Dr. Kimihiko Satoh (Hirosaki University School of Medicine, Hirosaki, Japan) provided probe for GSTπ (GSTP). DNA probes for UGT1A7 and total UGT1A were prepared by PCR using the following sets of primers: UGT1A7 sense primer, 5′-GCAGATGGTTGTGGAGAAACTC-3′; with antisense primer, 5′-GAGGTCTGTCATAGTCACTGG-3′; total UGT1A sense primer, 5′-AGCCTATGTCAACGCCTCTGG-3′; and with antisense primer, 5′-CCACTTCTCAATGGGTCTTGG-3′.

Establishment of Primary Cultures of Mouse Urothelial Cells. We adopted and modified the protocol to isolate bladder epithelium from male mice (42). Briefly, after the whole bladder was excised, it was everted to expose the mucosal surface. The bladder was digested in 20 units of dispase (Life Technologies, Inc., Rockville, MD) in PBS for 1 hour at 37°C. Following digestion, the bladder mucosa was gently detached from the underlying muscle tissue using fine-toothed forceps with coarse tips under a dissecting microscope. Mucosa was collected in PBS and further digested with 0.15% trypsin/EDTA at 37°C for 5 to 10 minutes. Trypsinized cells were mechanically dissociated by rigorous pipetting, filtered through a 100-μm nylon cloth, and centrifuged at 200 × *g* for 5 minutes. Approximately 5 to 10 × 10^5 cells were seeded in a 50-mm plastic dish containing a 1:1 mixture of serum-free keratinocyte medium and DMEM with 5% (v/v) fetal bovine serum, epidermal growth factor (5 ng/mL), bovine pituitary extract (50 μg/mL), cholera toxin (30 ng/mL), penicillin (100 units/mL), and streptomycin (1 μg/mL). The reagents used for this culture experiment were from Life Technologies.

Immunoblot Analysis. The nuclei of mouse hepatic cells and primary mouse urothelial cells prepared as described previously were solubilized with SDS-sample buffer without loading dye and 2-mercaptoethanol. Protein concentrations were estimated by BCA protein assay (Pierce, Rockford, IL). Proteins were separated by 6.0% SDS-PAGE and electrotransferred onto an Immobilon membrane (Millipore, Bedford, MA). Anti-Nrf2 antibody was used as described previously (32). Drs. Shigeru Taketani (Kyoto Institute of Technology, Kyoto, Japan) and John Hayes (University of Dundee, Dundee, United Kingdom) provided anti-heme oxygenase 1 (HO-1) and anti-GSTA1/A2 antibodies, respectively. Immunoreactive proteins were detected using horseradish peroxidase-conjugated anti-IgG antibody and enhanced chemiluminescence (Amersham Biosciences, Piscataway, NJ).

Determination of BCPN. The urinary level of BCPN was determined as reported previously (43) with modification. The urine sample (0.1 mL) was diluted to 0.5 mL with distilled water before assay. A 3.3-μL aliquot of 12 mol/L HCl was added, and the sample was extracted with 0.5 mL of ethyl acetate three times. The organic layers were collected after centrifugation for 5 minutes at 10,000 × *g* and dried using a speed vacuum concentrator with a cooling trap <30°C. The residues dissolved in ethyl acetate were spotted onto a silica gel 70 F_{254} precoated plate (Wako, Osaka, Japan) and developed with chloroform/methanol/acetic acid (18:1:1, v/v) in the dark. The bands corresponding to BBN or BCPN (Rf = 0.68 to 0.72) were scraped off and eluted from the silica with 4 mL acetone. The eluates then were concentrated by speed vacuum as before and diluted with acetonitrile to a final volume of 0.2 mL. Samples were filtered through a MINISART RC4 filter (0.2-μm pore size; Sartorius, Gottingen, Germany) and analyzed by high-performance liquid chromatography (HPLC). The urinary BCPN level was determined with a Shimazu LC9A apparatus (Shimazu, Kyoto, Japan) on a Finepak SIL C_{18} column (Jasco, Tokyo, Japan; 250 × 4.6 mm, inner diameter) at 239 nm. Separation was performed with a mobile phase consisting of a 3:7 mixture

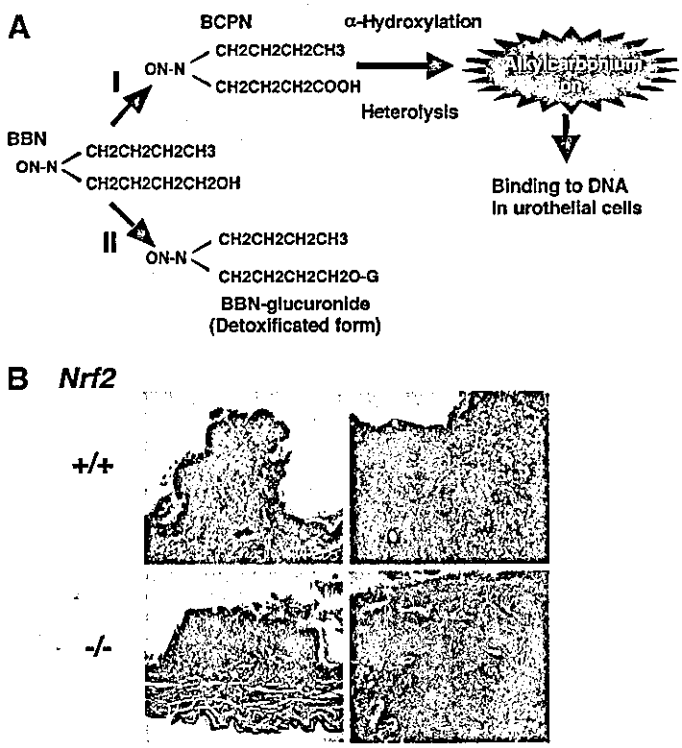

Fig. 1. BBN-induced carcinogenesis in wild-type and *Nrf2*$^{-/-}$ mouse urinary bladders. *A*, biotransformation processes of BBN; *G*, glucuronic acid. *B*, histopathologic analysis of tumor regions. Tissue sections of urinary bladder from wild-type (*top*) and *Nrf2*$^{-/-}$ (*bottom*) mice were analyzed by H&E staining. Noninvasive carcinoma (*left*) and invasive carcinoma (*right*) are shown.

Table 1 *BBN-induced carcinogenesis of the urinary bladder in wild-type and Nrf2$^{-/-}$ male mice and effect of oltipraz on the carcinogenesis*

Genotype	Oltipraz treatment	Cancer incidence Number (%)	Invasive cancer incidence Number (%)	Total number (entry number)
Wild type	−	9 (36.0)	6 (24.0)	25 (26)
	+	4 (13.8)	1 (3.4)*	29 (29)
Nrf2−/−	−	17 (65.4)*	10 (38.5)	26 (27)
	+	15 (65.2)*	6 (26.1)	22 (26)

* $P < 0.05$ compared with untreated wild-type mice.

(v/v) of acetonitrile and 20 mmol/L sodium acetate buffer (pH 4.5) at a flow rate of 1 mL/min. Under these conditions, the retention time of BCPN was 7.8 minutes. The recovery rate of BCPN from the urine was ~60% in our assay conditions.

Measurement of BBN-Glucuronide *In vitro*. Microsomes were prepared from mouse liver as described previously (44). A typical reaction mixture consisted of 100 mmol/L potassium phosphate buffer (pH 7.4), 1 mmol/L BBN, 5 mmol/L UDPGA, 0.05% Brij 58, and microsome preparation (600 μg) in a final volume of 1.0 mL. Reactions were initiated by the addition of BBN, and incubations were performed at 37°C for 30 minutes. BSA (1 mg) and 24% trichloroacetic acid (0.1 mL) were added to the incubation mixture to terminate the reaction. After centrifugation at 10,000 × *g* for 5 minutes, the supernatant (0.1 mL) was injected into the HPLC as described previously. Separation of BBN and its glucuronide was carried out with a mobile phase consisting of a 2:8 mixture (v/v) of acetonitrile and 20 mmol/L sodium acetate buffer (pH 4.5) at a flow rate of 1 mL/min.

Statistical Analyses. Data were expressed as mean ± SEM. The Student *t* test was used to determine the statistical difference among groups. The values for urinary bladder incidence were analyzed using the χ^2 or Fisher's exact probability test. A P value < 0.05 was accepted as statistically significant.

RESULTS

High Susceptibility of *Nrf2*$^{-/-}$ Mice to BBN-Induced Carcinogenesis. BBN is metabolized primarily through two pathways (45): one is alcohol/aldehyde dehydrogenase-mediated oxidation to yield BCPN, whereas the other is UGT-catalyzed conjugation to form BBN-glucuronide (Fig. 1; pathways I and II, respectively). Because glucuronide conjugation is an important process for detoxifying reactive chemicals, it has been suggested that a change in the distribution of BBN metabolites, such as a decrease in BCPN or an increase in BBN-glucuronide, might affect the incidence of tumor formation during exposure to BBN.

To elucidate the roles of Nrf2 in the prevention of urinary bladder carcinogenesis by BBN, we examined the susceptibility of *Nrf2*$^{-/-}$ mice to BBN carcinogenesis. Although *Nrf2*$^{-/-}$ mice were slightly heavier (<2.0 g) than wild-type animals, there was no significant difference in the body weight gained between the two groups during the experimental period. Several mice died before the end of the experiment (Table 1). In the group of wild-type mice, one mouse died within the experimental period, and its death was not attributable to BBN treatment. Conversely, five mice from the group of *Nrf2*$^{-/-}$ died before the end of the experiment. Autopsy revealed abdominal masses

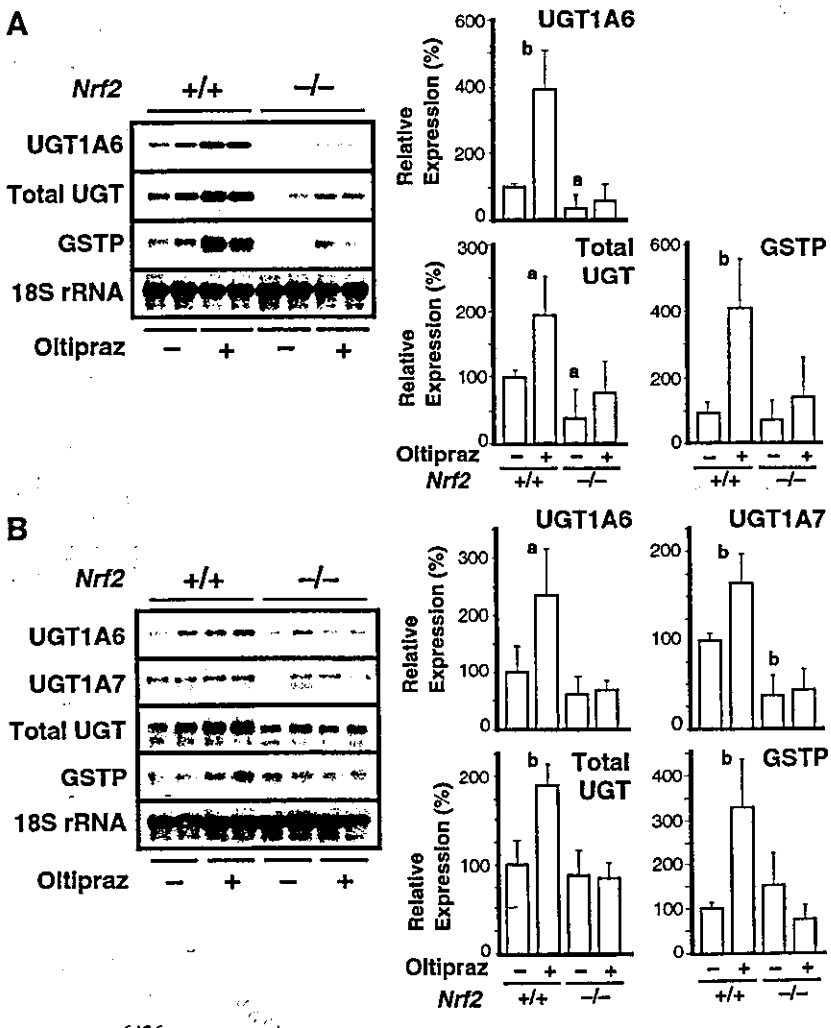

Fig. 2. Effect of oltipraz on the expression of phase 2 enzyme mRNAs in the liver and urinary bladder. *A* and *B*, effect of oltipraz on the expression of phase 2 enzyme genes in the liver (*A*) and urinary bladder (*B*) in wild-type and *Nrf2*$^{-/-}$ male mice. Oltipraz was fed at the concentration of 1 g/kg diet for 48 hours. Densitometric data of RNA blot analysis were normalized by 18S rRNA and expressed as ratios to vehicle-treated controls. Values are represented as mean ± SE ($n = 4$). *a*, $P \leq 0.05$ compared with nontreated wild-type mice. *b*, $P \leq 0.01$ compared with nontreated wild-type mice.

involving kidney and lymph nodes in three of these dead mice, apparently attributable to the BBN treatment. Bladder lesions were diagnosed histologically according to the previously described criteria (41). All of the noninvasive carcinomas were nodular rather than papillary in shape. The term "cancer" has been applied to transitional and squamous cell carcinomas because most of the lesions contained both components. No pathologic differences in noninvasive (Fig. 1*B*, *top* and *bottom left*) and invasive tumors (Fig. 1*B*, *top* and *bottom right*) were found between wild-type and *Nrf2*$^{-/-}$ mice, respectively.

Table 1 summarizes the incidence of urinary bladder cancer caused by BBN treatment. The incidence of noninvasive and invasive carcinoma was significantly higher in *Nrf2*$^{-/-}$ mice (65.4%) than in wild-type mice (36.0%; $P = 0.036$). In BBN-treated mice, invasive carcinoma was found in 38.5% and 24.0% of *Nrf2*$^{-/-}$ and wild-type mice, respectively. In wild-type mice, oltipraz treatment reduced the incidence of urinary bladder cancer by 61.6% and the incidence of invasive cancer by 85% ($P = 0.041$). However, in *Nrf2*$^{-/-}$ mice, oltipraz significantly lost its chemopreventive efficacy, although oltipraz partially reduced the incidence of invasive cancer. These results clearly indicate that detoxifying enzymes under Nrf2 regulation contribute to the cancer chemopreventive effect of oltipraz.

Expression of Phase 2 Genes in the Liver and Urinary Bladder of *Nrf2*$^{-/-}$ and Wild-Type Mice Treated with Oltipraz. To elucidate the roles that Nrf2 may play in the protection against BBN carcinogenesis afforded by oltipraz, we examined changes in the expression of detoxifying enzyme genes in the liver and urinary bladder following oltipraz treatment. For this purpose, oltipraz (1 g/kg) was added to the diet and fed to mice for 48 hours. The mRNA levels of UGT1A6, total UGT1A, and GSTP were monitored by RNA blot analysis. The constitutive expression of these detoxifying genes was 40 to 50% lower in the livers of *Nrf2*$^{-/-}$ mice than in wild-type mice (Fig. 2*A*). Although oltipraz increased the mRNA levels of UGT1A6 and GSTP by approximately fourfold and that of total UGT1A by twofold in the livers of wild-type mice, the inducible expression of these genes by oltipraz was markedly reduced in the livers of *Nrf2*$^{-/-}$ mouse (Fig. 2*A*).

Next, the expression profiles of these detoxifying enzyme genes in the urinary bladder were examined. We found that the basal level of these detoxifying enzyme mRNAs in the bladder were lower in *Nrf2*$^{-/-}$ mice than in wild-type mice (Fig. 2*B*). Oltipraz induced the expression of these enzymes in the urinary bladder of wild-type mice, but the magnitude of induction was less, approximately twofold for UGT1A6 and threefold for GSTP. The inducible expression of these genes by oltipraz was significantly abrogated in the *Nrf2*$^{-/-}$ mouse urinary bladder (Fig. 2*B*). We also examined the expression of UGT1A7 mRNA. UGT1A7 mRNA was detected in the urinary bladder (Fig. 2*B*) but not in the liver (data not shown), and the constitutive and inducible expressions were affected in the *Nrf2*$^{-/-}$ mouse urinary bladder. These results revealed that phase 2 detoxifying enzymes are expressed in the urinary bladder and that Nrf2 regulates their expression in response to electrophilic inducers.

Nrf2 Regulatory Pathway Is Activated in Liver and Urothelial Cells. We next examined Nrf2 activation by oltipraz in liver and urothelial cells. The mRNA levels of Nrf2 itself did not change substantially on treatment with oltipraz in either tissue (Fig. 3*A*). Because we carried out a targeting knockout of the *Nrf2* gene by introducing the β-galactosidase gene into the *Nrf2* locus, creating Nrf2–β-galactosidase fusion mRNA (30), we detected larger-sized mRNA in the *Nrf2*$^{-/-}$ mice. The level of the larger-sized mRNA did not change much on treatment with oltipraz (Fig. 3*A*). These observations are consistent with our contention that activation of Nrf2 correlates with nuclear accumulation of Nrf2 protein. To confirm this point further, we examined the nuclear expression of Nrf2 protein in

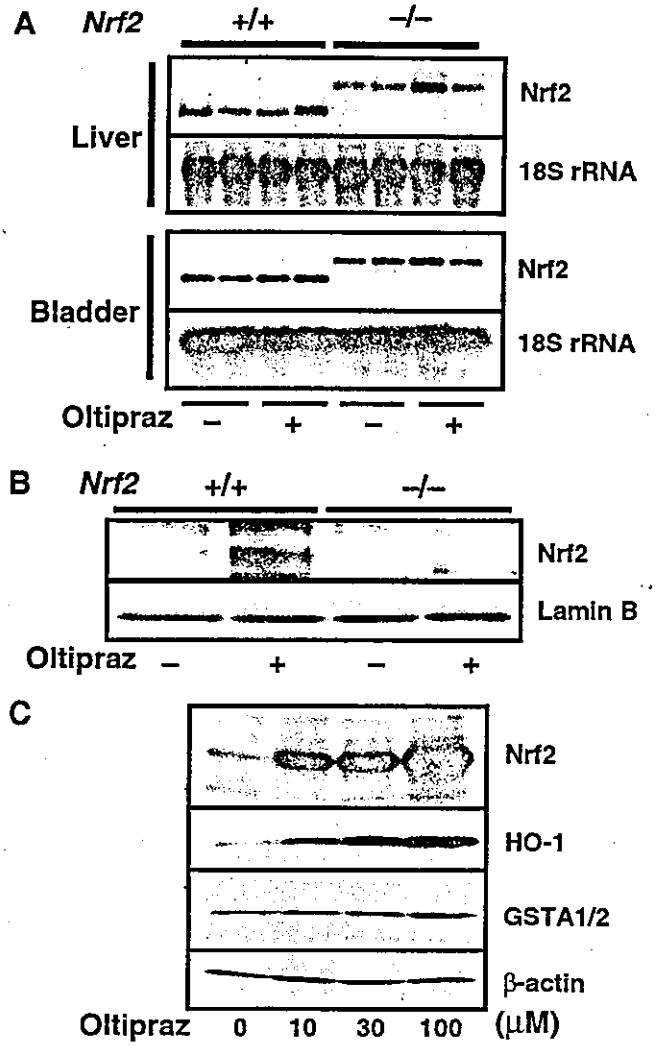

Fig. 3. Effect of oltipraz on Nrf2 activation in the liver and urinary bladder. *A*, effect of oltipraz on the expression of Nrf2 mRNA in the liver and urinary bladder of male wild-type and *Nrf2*$^{-/-}$ mice. Mice were fed oltipraz at the concentration of 1 g/kg diet for 48 hours. Densitometric analysis of RNA blot results was normalized by 18S rRNA levels and expressed as ratios to vehicle-treated controls. Values are represented as mean ± SE ($n = 4$). *B*, Nrf2 activation in mouse liver by oltipraz. Male wild-type and *Nrf2*$^{-/-}$ mice were fed oltipraz at the concentration of 1 g/kg diet for 48 hours, and hepatic nuclear extracts were examined by immunoblot analysis using anti-Nrf2 antibody. Lamin B was used as a loading control. *C*, immunoblot analyses of Nrf2, HO-1, and GSTA1/2 in mouse uroepithelial primary cell cultures. Total cell extract prepared from wild-type uroepithelial cells was treated with 10, 30, and 100 μmol/L oltipraz or vehicle for 8 hours. β-Actin was used as a loading control.

the liver after treatment with oltipraz. Immunoblot analysis showed an increased nuclear accumulation of Nrf2 protein in wild-type mice, but not in *Nrf2*$^{-/-}$ mice, following exposure to oltipraz (Fig. 3*B*).

To date, there have been no reports describing the expression of Nrf2 and its target genes in urothelial cells. However, the Nrf2-dependent expression of phase 2 enzyme genes in the urinary bladder suggests that the Nrf2 regulatory pathway is functioning in urothelial cells. We clarified that this is the case by establishing a primary urothelial cell culture system and examining the expression of Nrf2. Immunoblot analysis of total cell extracts with anti-Nrf2 antibody showed that the amount of Nrf2 protein is increased by oltipraz in a dose-dependent manner (Fig. 3*C*). Oltipraz also induced the nuclear accumulation of Nrf2 (data not shown) and the expressions of HO-1 and GSTA1/A2 (Fig. 3*C*).

Elevated BCPN Concentration in the Urine of *Nrf2*$^{-/-}$ Mice. BCPN is a proximate metabolite of BBN, and BCPN and BBN are metabolized through α-hydroxylation/spontaneous cleavage to pro-

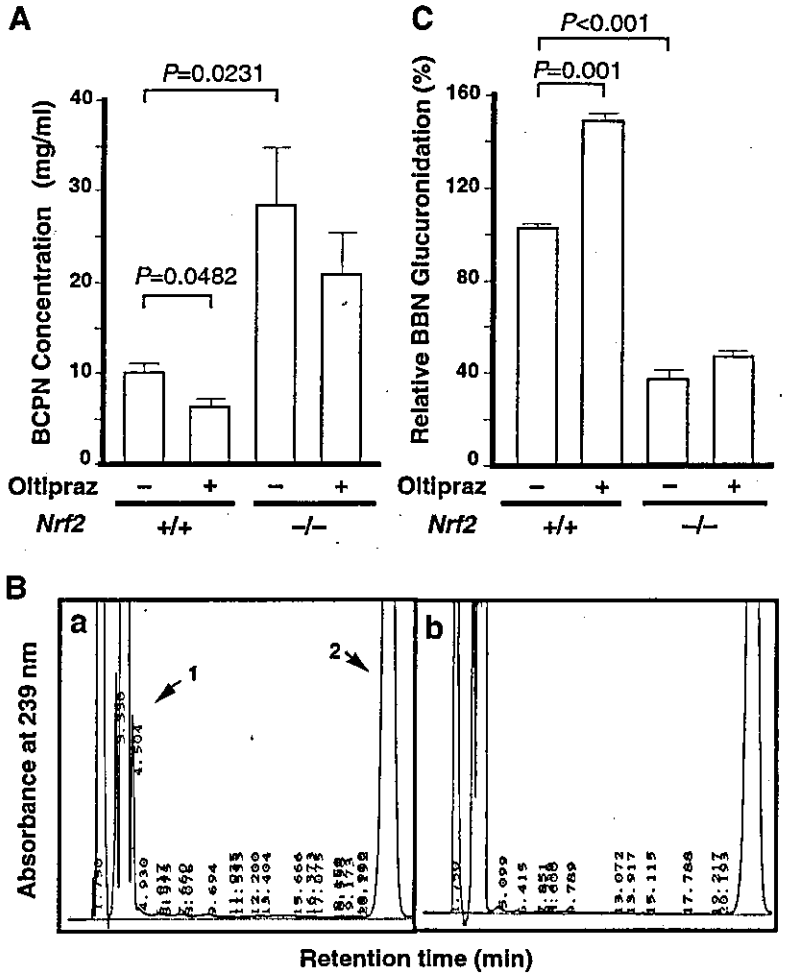

Fig. 4. Effect of *Nrf2* genotype and oltipraz treatment on the urinary concentration of BCPN after treatment with BBN and the activity of BBN glucuronidation in hepatic microsomes. *A*, Mice were fed 250 mg/kg diet of oltipraz and 0.05% BBN in drinking water for 2 weeks, and then urine samples were analyzed by HPLC. Values are represented as mean ± SE ($n = 5$). *Significantly different from nontreated wild-type mice ($P \leq 0.05$). *B*, Mice given oltipraz at the concentration of 250 mg/kg diet for 2 weeks were used. Hepatic microsomes from the animals were prepared as described in Materials and Methods. Six hundred micrograms of Brij 58-solubilized microsomes from mouse livers were incubated with 1 mmol/L BBN in the presence of 5 mmol/L UDPGA at 37°C for 30 minutes. *a*, complete system; *b*, without enzyme preparation. Peaks 1 and 2 were identified as BBN-glucuronide and BBN, respectively. *C*, The relative formation of BBN-glucuronide by liver microsomes from mice treated either with or without oltipraz treatment. Values are represented as mean ± SE ($n = 3$). *Significantly different from untreated wild-type mice ($P \leq 0.05$).

duce their alkylcarbonium ion. These reactive species can covalently bind to DNA and are associated with the formation of a butyl-guanine adduct in the urothelial DNA of animals treated with BBN (16). We hypothesized that increased carcinogenesis in $Nrf2^{-/-}$ mice is associated with a higher than normal urinary BCPN concentration. We measured by HPLC the urinary concentration of BCPN 2 weeks after administration of 0.05% BBN to mice treated either with or without oltipraz (Fig. 4*A*). Mice were fed oltipraz (250 mg/kg) 1 week before BBN administration. The urinary concentration of BCPN was significantly higher in $Nrf2^{-/-}$ mice than in wild-type mice ($P = 0.0231$). Oltipraz treatment significantly reduced the urinary concentration of BCPN in wild-type mice ($P = 0.0482$) but not in $Nrf2^{-/-}$ mice.

Oltipraz Enhanced BBN Glucuronidation Activity in Liver Microsomes. Considering that BBN glucuronidation occurs mainly in the liver, it is reasonable to assume that an increase in BBN glucuronidation in the liver would contribute, at least in part, to a decrease in BCPN concentration in the urine and consequent suppression of carcinogenesis in the urinary bladder. Therefore, we measured the glucuronidation activity of BBN in hepatic microsomes *in vitro* by HPLC. Incubation of BBN (peak 2) with the Brij 58-solubilized microsome of wild-type mouse liver in the presence of UDPGA resulted in a new product (peak 1) with a retention time of 4.5 minutes (Fig. 4*B*, *a*). This metabolite was not detected when the enzyme preparation (Fig. 4*B*, *b*), UGPGA (data not shown), or BBN (data not shown) was excluded from the incubation mixture, indicating that the product was BBN-glucuronide generated from BBN.

The basal activity of BBN glucuronidation was significantly lower in the hepatic microsomes of $Nrf2^{-/-}$ mice than in wild-type mice ($P = 0.001$). Oltipraz significantly induced the BBN glucuronidation activity in wild-type mouse liver microsomes ($P = 0.001$) but not in $Nrf2^{-/-}$ mouse liver microsomes (Fig. 4*C*). Collectively, these results suggest that the administration of oltipraz reduces the concentration of BCPN in the urine by enhancing the hepatic BBN glucuronidation activity.

BBN Decreases UGT Expression, and Oltipraz Counteracts the Suppression in Urinary Bladder. It was reported previously that *UGT1A* gene expression in cancerous human urinary bladder was either lost or decreased to a low level compared with that in normal bladder tissue (13). Such down-regulation of UGT expression in the urinary bladder may reduce the local glucuronidation activity of carcinogenic compounds, allowing their accumulation and promoting DNA mutations in the urinary bladder.

We analyzed the effect of BBN on *UGT1A* gene expression in the urinary bladder by supplementing drinking water with 0.01%, 0.05%, or 0.1% BBN for 2 weeks. The expressions of *UGT1A6*, *UGT1A7*, and total *UGT1A* were significantly decreased by BBN treatment in a dose-dependent manner (Fig. 5*A*). Importantly, this pattern of *UGT1A* suppression by BBN also was observed in $Nrf2^{-/-}$ mice (Fig. 5*B*). We tested whether oltipraz counteracts the down-regulation of *UGT1A* gene expression by BBN. Mice were given 250 mg/kg of oltipraz in the diet 1 week before carcinogen administration (0.01% BBN) in the drinking water for 2 weeks. In wild-type mice, BBN decreased the expressions of *UGT1A6*, *UGT1A7*, and total *UGT1A* by 50.1%, 54.0%, and 52.0%, respectively, whereas in $Nrf2^{-/-}$ mice, BBN markedly reduced the expressions of *UGT1A6*, *UGT1A7*, and total *UGT1A* to <10% (Fig. 5*A* and *C*). Oltipraz effectively inhibited

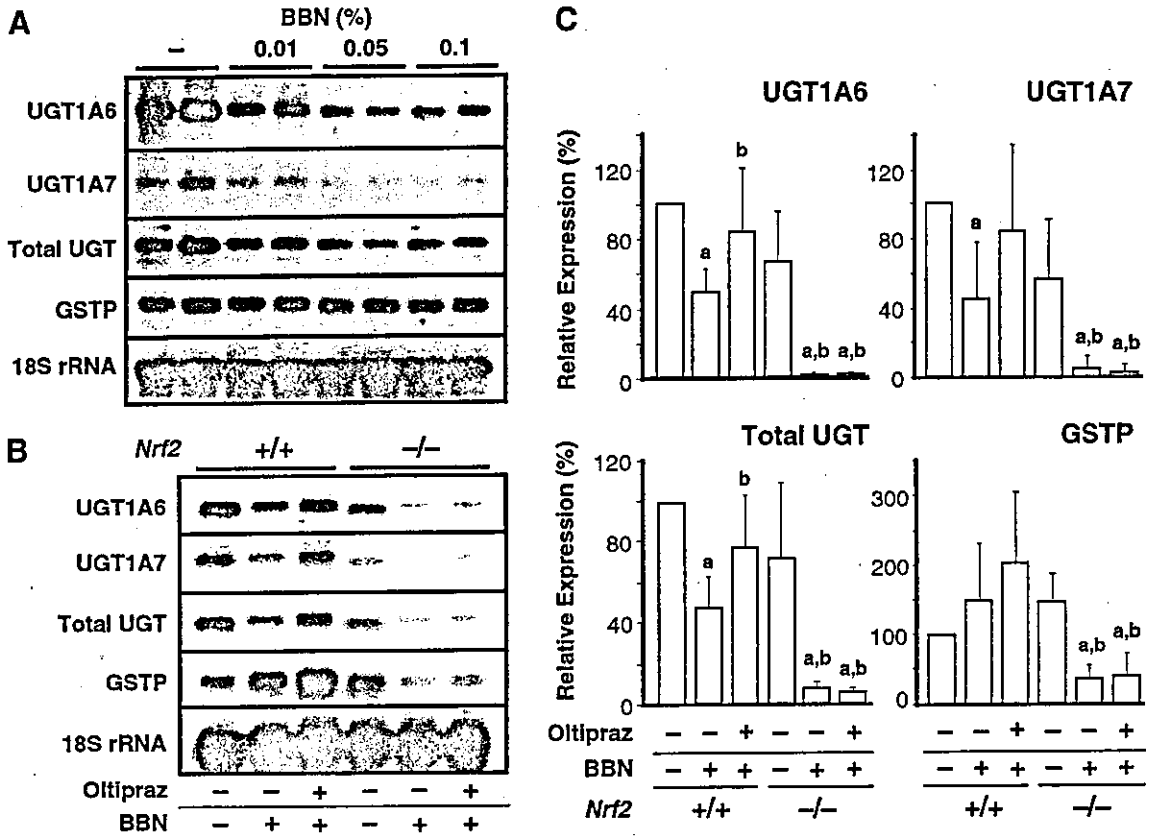

Fig. 5. Effect of BBN and oltipraz on the expressions of phase 2 genes. *A*, effect of BBN on the expressions of phase 2 genes in the urinary bladder of male wild-type mice. Mice were treated with 0.01%, 0.05%, 0.1% BBN, or vehicle in drinking water for 2 weeks. *B*, The expressions of phase 2 genes after BBN and oltipraz treatment were examined in wild-type and $Nrf2^{-/-}$ mice. Oltipraz was fed at the concentration of 250 mg/kg diet 1 week before carcinogen administration. BBN was given at a concentration of 0.01% in drinking water for 2 weeks. *C*, Densitometric analysis of RNA blot results was normalized by 18S rRNA levels and expressed as ratios to vehicle-treated controls. Values are represented as mean ± SE ($n = 4$). *a*, $P \leq 0.05$ compared with nontreated wild-type mice. *b*, $P \leq 0.05$ compared with BBN-treated wild-type mice.

the down-regulation of *UGT1A* genes caused by BBN in the urinary bladder of wild-type mice but completely lost its efficacy in $Nrf2^{-/-}$ mice (Fig. 5*B* and *C*). BBN did not suppress *GSTP* gene expression, indicating that BBN specifically targets *UGT1A* genes (Fig. 5). Thus, these results show that BBN suppresses *UGT1A* gene expression in the urinary bladder through mechanisms independent of the Nrf2 regulatory pathway.

DISCUSSION

Our study has shown that $Nrf2^{-/-}$ mice are more susceptible to BBN-induced carcinogenesis of the urinary bladder than wild-type mice. The elevated incidence of BBN carcinogenesis in $Nrf2^{-/-}$ mice was associated with the higher concentration of BCPN in the urine and lower activity of BBN-glucuronidation in the liver. Whereas oltipraz effectively reduced the incidence of urinary bladder carcinoma initiated by BBN in wild-type C57BL/6 mice, it showed little effect in $Nrf2^{-/-}$ mice. In wild-type mice, oltipraz significantly increased the activity of BBN-glucuronidation in the liver, an increase that correlated well with the increased *UGT1A* gene expression, and thereby reduced the urinary concentration of BCPN. Furthermore, oltipraz increased the expression of phase 2 enzyme genes and suppressed the BBN-induced down-regulation of *UGT1A* expression in urinary bladder in an Nrf2-dependent manner. Collectively, these results highlight the importance of a set of detoxifying and cytoprotective enzymes under the regulatory influence of Nrf2 in the prevention of urothelial carcinogenesis.

Epidemiologic and experimental lines of evidence also suggest that the activity of detoxifying enzymes is tightly linked to urinary bladder carcinogenesis. However, the mechanism as to how the decrease in detoxifying enzyme activity contributes to carcinogenesis of the urinary bladder remains to be clarified. It was reported previously that oltipraz, an inducer of phase 2 detoxifying enzymes, reduces the incidence of bladder cancer caused by BBN (46). Exploiting $Nrf2^{-/-}$ mice for the BBN-carcinogenesis experiment, this study proved that oltipraz acts to prevent the initiation of cancer through activation of detoxification enzymes under Nrf2 regulation. It is of note that oltipraz repressed the incidence of invasive cancer and urinary BCPN concentration even in $Nrf2^{-/-}$ mice, indicating that oltipraz exerts its chemopreventive function partially through a pathway independent of Nrf2. Oltipraz was reported to induce *GSTA2* gene expression by activating CAAT/enhancer binding protein β (47).

One salient observation in this study was that the detoxification processes in the liver and urinary bladder act simultaneously and cooperatively to prevent chemical carcinogenesis of the urinary bladder. Our current model for the roles of Nrf2 and its downstream gene products in protection against BBN carcinogenesis is summarized in Fig. 6. In this model, oltipraz prevents BBN carcinogenesis primarily through the induction of BBN glucuronidation in the liver. Oltipraz also induces phase 2 and antioxidant enzymes in the urinary bladder in an Nrf2-dependent manner. Because BBN and BCPN are metabolized to reactive species in urothelial cells, it is likely that the defense system in the urinary bladder plays a key role in the anticarcinogenic mechanism (16). Therefore, induction of Nrf2-mediated detoxifying enzymes in the peripheral urothelial cells and in liver may become an important strategy to prevent BBN-induced bladder carcinogenesis.

It has been shown that decreased expression of phase 2 detoxifying

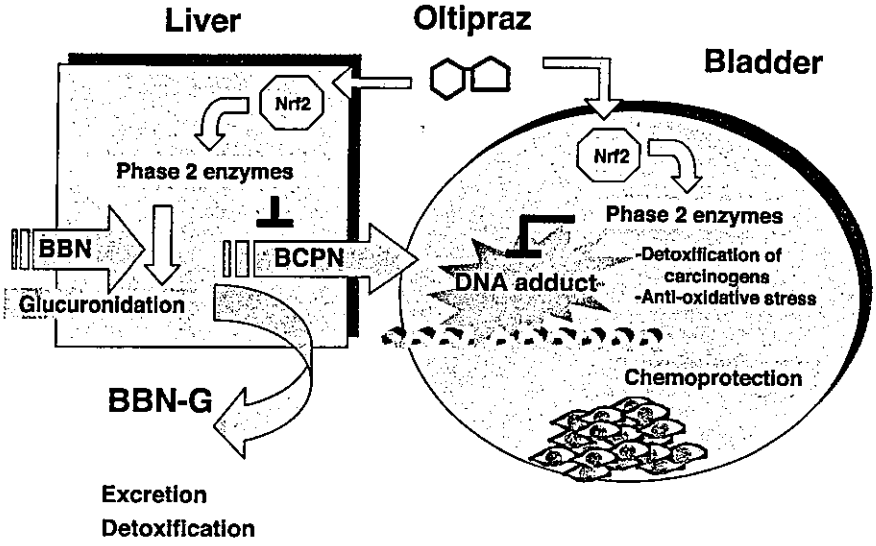

Fig. 6. Mechanism of chemoprotection by oltipraz against urinary bladder carcinogenesis. Oltipraz reduced BBN-induced carcinogenesis by suppressing the urinary excretion of BCPN by means of Nrf2-dependent induction of BBN glucuronidation in the liver. Moreover, oltipraz also works in the urinary bladder by inducing phase 2 enzymes and antioxidant proteins, such as HO-1, to suppress BBN-induced carcinogenesis. Furthermore, oltipraz counteracted the BBN-provoked urinary bladder-specific suppression of *UGT1A* gene expression in an Nrf2-dependent manner.

enzymes predisposes cells to neoplastic transformation. For example, Nelson *et al.* (48) reported that the loss of *GSTP1* expression in the prostate precedes neoplastic transformation. Expression of the *GSTP1* gene, which is the major GST isoform expressed in normal human prostate, is silenced in the majority of prostate tumors by the hypermethylation of CpG islands residing in the 5′ regulatory region. Conversely, overexpression of *GSTP1* in the prostate cell line LNCaP inhibited the cytotoxicity and DNA-adduct formation caused by a potential dietary carcinogen (49). Down-regulation of *UGT1A* gene expression also was found in an early stage of hepatocarcinogenesis (50).

In the case of urinary bladder cancer, it has been reported that carcinogenesis is associated with a decrease in or loss of *UGT1A* gene expression (13). Therefore, the finding that BBN acts to repress *UGT1A* gene expression in a urinary bladder-specific manner is intriguing. We found in this study that BBN significantly decreases *UGT1A* gene expression in a dose-dependent manner and that this decrease is observed as early as 1 day after administration of BBN (data not shown). This down-regulation of *UGT1A* leads to increased BBN or BCPN levels in urothelial cells, which may ultimately increase DNA alkylation. These observations also suggest the presence of bladder-specific regulation of *UGT1A* gene expression, which is sensitive to BBN. Because suppression also was observed in *Nrf2*$^{-/-}$ mice, the mechanism seems to be independent of Nrf2 regulation. In contrast, oltipraz counteracted the BBN-induced suppression in an Nrf2-dependent manner, suggesting that expression of *UGT1A* genes is under multiple regulatory influences. The Nrf2 regulatory pathway may compensate for the BBN-induced down-regulation of *UGT1A* gene expression in wild-type mice.

It was reported that *p53* gene knockout mice (*p53*$^{+/-}$ mice) are susceptible to BBN-induced urinary bladder carcinogenesis (43). The high susceptibility of *p53*$^{+/-}$ mice to BBN was associated with an increased cell proliferation without alteration of BCPN concentration in the urine. If we consider the high level of BCPN in the urine of *Nrf2*$^{-/-}$ mice, the mechanism that makes *Nrf2*$^{-/-}$ mice susceptible to BBN carcinogenesis must be different from that observed in *p53*$^{+/-}$ mice. Therefore, the use of a combination of oltipraz and other chemopreventive agents with distinct molecular targets would provide a strong synergistic efficacy. An attractive prospect also would be the discovery of more powerful chemical agents that are specifically delivered to the urinary bladder to induce the expression of phase 2 enzyme genes. Such strategies may be of importance in the protection against urinary bladder carcinogenesis.

ACKNOWLEDGMENTS

We thank Drs. Yukio Mori, Shigeru Taketani, John D. Hayes, Kimihiko Satoh, Shoji Fukushima, and Kit Tong for discussion and advice.

REFERENCES

1. Wai CY, Miller DS. Urinary bladder cancer. Clin Obstet Gynecol 2002;45:844–54.
2. Case RA, Hosker ME, McDonald DB, Pearson JT. Tumours of the urinary bladder in workmen engaged in the manufacture and use of certain dyestuff intermediates in the British chemical industry. Part I. The role of aniline, benzidine, α-naphthylamine, and β-naphthylamine. Br J Ind Med 1954;11:75–96.
3. Tricker AR, Mostafa MH, Spiegelhalder B, Preussmann R. Urinary excretion of nitrate, nitrite and N-nitroso compounds in schistosomiasis and bilharzia bladder cancer patients. Carcinogenesis 1989;10:547–52.
4. Mirvish SS. Role of N-nitroso compounds (NOC) and N-nitrosation in etiology of gastric, esophageal, nasopharyngeal and bladder cancer and contribution to cancer of known exposures to NOC. Cancer Lett 1995;93:17–48.
5. Druckrey H, Preussmann R, Ivankovic S, Schmahl D. Organotropic carcinogenic effects of 65 various N-nitroso- compounds on BD rats. Z Krebsforsch 1967;69:103–201.
6. IARC. N-Nitrosodi-n-butylamine. IARC Monogr Eval Carcinog Risk Chem Man 1978;17:51–75.
7. Okada M, Ishidate M. Metabolic fate of N-n-butyl-N-(4-hydroxybutyl)-nitrosamine and its analogues. Selective induction of urinary bladder tumours in the rat. Xenobiotica 1977;7:11–24.
8. Ito N, Hiasa Y, Tamai A, Okajima E, Kitamura H. Histogenesis of urinary bladder tumors induced by N-butyl-N-(4-hydroxybutyl)nitrosamine in rats. Gann 1969;60:401–10.
9. Brockmoller J, Cascorbi I, Kerb R, Roots I. Combined analysis of inherited polymorphisms in arylamine N-acetyltransferase 2, glutathione S-transferases M1 and T1, microsomal epoxide hydrolase, and cytochrome P450 enzymes as modulators of bladder cancer risk. Cancer Res 1996;56:3915–25.
10. Johns LE, Houlston RS. N-acetyl transferase-2 and bladder cancer risk: a meta-analysis. Environ Mol Mutagen 2000;36:221–7.
11. Johns LE, Houlston RS. Glutathione S-transferase 11 (GSTM1) status and bladder cancer risk: a meta-analysis. Mutagenesis 2000;15:399–404.
12. Park SJ, Zhao H, Spitz MR, Grossman HB, Wu X. An association between NQO1 genetic polymorphism and risk of bladder cancer. Mutat Res 2003;536:131–7.
13. Giuliani L, Gazzaniga P, Caporuscio F, Ciotti M, Frati L, Agliano AM. Can down-regulation of UDP-glucuronosyltransferases in the urinary bladder tissue impact the risk of chemical carcinogenesis? Int J Cancer 2001;91:141–3.
14. Hashimoto Y, Kitagawa HS. In vitro neoplastic transformation of epithelial cells of rat urinary bladder by nitrosamines. Nature 1974;252:497–99.
15. Airoldi L, Magagnotti C, Bonfanti M, Fanelli R. α-Oxidative metabolism of the bladder carcinogens N-nitrosobutyl(4-hydroxybutyl)amine and N-nitrosobutyl(3-carboxypropyl)-amine within the rat isolated bladder. Carcinogenesis 1990;11:1437–40.
16. Airoldi L, Magagnotti C, Bonfanti M, et al. Detection of O6-butyl- and O6-(4-hydroxybutyl)guanine in urothelial and hepatic DNA of rats given the bladder carcinogen N-nitrosobutyl(4-hydroxybutyl)amine. Carcinogenesis 1994;15:2297–301.
17. Talalay P. Chemoprotection against cancer by induction of phase 2 enzymes. Biofactors 2000;12:5–11.
18. Talalay P, Dinkova-Kostova AT, Holtzclaw WD. Importance of phase 2 gene regulation in protection against electrophile and reactive oxygen toxicity and carcinogenesis. Adv Enzyme Regul 2003;43:121–34.
19. Benson AM, Batzinger RP, Ou SY, Bueding E, Cha YN, Talalay P. Elevation of hepatic glutathione S-transferase activities and protection against mutagenic metabolites of benzo(a)pyrene by dietary antioxidants. Cancer Res 1978;38:4486–95.

20. Ansher SS, Dolan P, Bueding E. Biochemical effects of dithiolethiones. Food Chem Toxicol 1986;24:405–15.
21. Zhang Y, Talalay P, Cho CG, Posner GH. A major inducer of anticarcinogenic protective enzymes from broccoli: isolation and elucidation of structure. Proc Natl Acad Sci USA 1992;89:2399–403.
22. Clapper ML. Chemopreventive activity of oltipraz. Pharmacol Ther 1998;78:17–27.
23. Kensler TW, Groopman JD, Sutter TR, Curphey TJ, Roebuck BD. Development of cancer chemopreventive agents: oltipraz as a paradigm. Chem Res Toxicol 1999;12: 113–26.
24. Primiano T, Sutter TR, Kensler TW. Antioxidant-inducible genes. Adv Pharmacol 1997;38:293–328.
25. Friling RS, Bensimon S, Daniel V. Xenobiotic-inducible expression of murine glutathione S-transferase Ya subunit gene is controlled by an electrophile-responsive element. Proc Natl Acad Sci USA 1990;87:6258–62.
26. Rushmore TH, Morton MR, Pickett CB. The antioxidant responsive element. J Biol Chem 1991;266:11632–9.
27. Itoh K, Igarashi K, Hayashi N, Nishizawa M, Yamamoto M. Cloning and characterization of a novel erythroid cell-derived CNC family transcription factor heterodimerizing with the small maf family proteins. Mol Cell Biol 1995;15:4184–93.
28. Moi P, Chan K, Asunis I, Cao A, Kan YW. Isolation of NF-E2-related factor 2 (Nrf2), a NF-E2-like basic leucine zipper transcriptional activator that binds to the tandem NF-E2/AP1 repeat of the α-globin locus control region. Proc Natl Acad Sci USA 1994;91:9926–30.
29. Venugopal R, Jaiswal AK. Nrf1 and Nrf2 positively and c-Fos and Fra1 negatively regulate the human antioxidant response element-mediated expression of NAD(P)H: quinone oxidoreductase1 gene. Proc Natl Acad Sci USA 1996;93:14960–5.
30. Itoh K, Chiba T, Takahashi S, et al. An Nrf2/small Maf heterodimer mediates the induction of phase II detoxifying enzyme genes through antioxidant response elements. Biochem Biophys Res Commun 1997;236:313–22.
31. Chan K, Lu R, Chang JC, Kan YW. NRF2, a member of the NFE2 family of transcription factors, is not essential for murine erythropoiesis, growth, and development. Proc Natl Acad Sci USA 1996;93:13943–8.
32. Ishii T, Itoh K, Takahashi S, et al. Transcription factor Nrf2 coordinately regulates a group of oxidative stress-inducible genes in macrophages. J Biol Chem 2000;275: 16023–9.
33. Ramos-Gomez M, Kwak MK, Dolan PM, et al. Sensitivity to carcinogenesis is increased and chemoprotective efficacy of enzyme inducers is lost in nrf2 transcription factor-deficient mice. Proc Natl Acad Sci USA 2001;98:3410–5.
34. Ramos-Gomez M, Dolan PM, Itoh K, Yamamoto M, Kensler TW. Interactive effects of nrf2 genotype and oltipraz on benzo[a]pyrene-DNA adducts and tumor yield in mice. Carcinogenesis 2003;24:461–7.
35. Fahey JW, Haristoy X, Dolan PM, et al. Sulforaphane inhibits extracellular, intracellular, and antibiotic-resistant strains of Helicobacter pylori and prevents benzo-[a]pyrene-induced stomach tumors. Proc Natl Acad Sci USA 2002;99:7610–5.
36. Chan K, Han XD, Kan YW. An important function of Nrf2 in combating oxidative stress: detoxification of acetaminophen. Proc Natl Acad Sci USA 2001;98:4611–6.
37. Enomoto A, Itoh K, Nagayoshi E, et al. High sensitivity of Nrf2 knockout mice to acetaminophen hepatotoxicity associated with decreased expression of ARE-regulated drug metabolizing enzymes and antioxidant genes. Toxicol Sci 2001;59: 169–77.
38. Chan K, Kan YW. Nrf2 is essential for protection against acute pulmonary injury in mice. Proc Natl Acad Sci USA 1999;96:12731–6.
39. Cho HY, Jedlicka AE, Reddy SP, et al. Role of NRF2 in protection against hyperoxic lung injury in mice. Am J Respir Cell Mol Biol 2002;26:175–82.
40. Aoki Y, Sato H, Nishimura N, Takahashi S, Itoh K, Yamamoto M. Accelerated DNA adduct formation in the lung of the Nrf2 knockout mouse exposed to diesel exhaust. Toxicol Appl Pharmacol 2001;173:154–60.
41. Oyasu R, Iwasaki T, Matsumoto M, Hirao Y, Tabuchi Y. Induction of tumors in heterotopic bladder by topical application of N-methyl-N-nitrosourea and N-butyl-N-(3-carboxypropyl)nitrosamine. Cancer Res 1978;38:3019–25.
42. Zhang YY, Ludwikowski B, Hurst R, Frey P. Expansion and long-term culture of differentiated normal rat urothelial cells in vitro. In Vitro Cell Dev Biol Anim 2001;37:419–29.
43. Ozaki K, Sukata T, Yamamoto S, et al. High susceptibility of p53(+/−) knockout mice in N-butyl-N-(4-hydroxybutyl)nitrosamine urinary bladder carcinogenesis and lack of frequent mutation in residual allele. Cancer Res 1998;58:3806–11.
44. Kumagai Y, Lin LY, Hiratsuka A, et al. Participation of cytochrome P450–2B and -2D isozymes in the demethylenation of methylenedioxymethamphetamine enantiomers by rats. Mol Pharmacol 1994;45:359–65.
45. Bonfanti M, Magagnotti C, Bonati M, Fanelli R, Airoldi L. Pharmacokinetic profile and metabolism of N-nitrosobutyl-(4-hydroxybutyl)amine in rats. Cancer Res 1988; 48:3666–9.
46. Moon RC, Kelloff GJ, Detrisac CJ, Steele VE, Thomas CF, Sigman CC. Chemoprevention of OH-BBN-induced bladder cancer in mice by oltipraz, alone and in combination with 4-HPR and DFMO. Anticancer Res 1994;14:5–11.
47. Kang KW, Cho IJ, Lee CH, Kim SG. Essential role of phosphatidylinositol 3-kinase-dependent CCAAT/enhancer binding protein beta activation in the induction of glutathione S-transferase by oltipraz. J Natl Cancer Inst 2003;95:53–66.
48. Nelson CP, Kidd LC, Sauvageot J, et al. Protection against 2-hydroxyamino-1-methyl-6-phenylimidazo[4,5-b]pyridine cytotoxicity and DNA adduct formation in human prostate by glutathione S-transferase P1. Cancer Res 2001;61:103–9.
49. Nelson WG, De Marzo AM, Deweese TL, et al. Preneoplastic prostate lesions: an opportunity for prostate cancer prevention. Ann NY Acad Sci 2001;952:135–44.
50. Strassburg CP, Manns MP, Tukey RH. Differential down-regulation of the UDP-glucuronosyltransferase 1A locus is an early event in human liver and biliary cancer. Cancer Res 1997;57:2979–85.

Genetic ablation of Nrf2 enhances susceptibility to cigarette smoke–induced emphysema in mice

Tirumalai Rangasamy,[1] Chung Y. Cho,[2] Rajesh K. Thimmulappa,[1] Lijie Zhen,[2] Sorachai S. Srisuma,[1] Thomas W. Kensler,[1,3] Masayuki Yamamoto,[4] Irina Petrache,[5] Rubin M. Tuder,[2,5] and Shyam Biswal[1,3]

[1]Department of Environmental Health Sciences, Bloomberg School of Public Health, [2]Department of Pathology, School of Medicine, [3]Department of Oncology, Sidney Kimmel Comprehensive Cancer Center, Johns Hopkins University, Baltimore, Maryland, USA. [4]Center for Tsukuba Advanced Research Alliance and Institute of Basic Medical Sciences, University of Tsukuba, Tsukuba, Japan. [5]Division of Pulmonary and Critical Care Medicine, Department of Medicine, School of Medicine, Johns Hopkins University, Baltimore, Maryland, USA.

Although inflammation and protease/antiprotease imbalance have been postulated to be critical in cigarette smoke–induced (CS-induced) emphysema, oxidative stress has been suspected to play an important role in chronic obstructive pulmonary diseases. Susceptibility of the lung to oxidative injury, such as that originating from inhalation of CS, depends largely on its upregulation of antioxidant systems. Nuclear factor, erythroid-derived 2, like 2 (Nrf2) is a redox-sensitive basic leucine zipper protein transcription factor that is involved in the regulation of many detoxification and antioxidant genes. Disruption of the *Nrf2* gene in mice led to earlier-onset and more extensive CS-induced emphysema than was found in wild-type littermates. Emphysema in *Nrf2*-deficient mice exposed to CS for 6 months was associated with more pronounced bronchoalveolar inflammation; with enhanced alveolar expression of 8-oxo-7,8-dihydro-2′-deoxyguanosine, a marker of oxidative stress; and with an increased number of apoptotic alveolar septal cells — predominantly endothelial and type II epithelial cells — as compared with wild-type mice. Microarray analysis identified the expression of nearly 50 Nrf2-dependent antioxidant and cytoprotective genes in the lung that may work in concert to counteract CS-induced oxidative stress and inflammation. The responsiveness of the Nrf2 pathway may act as a major determinant of susceptibility to tobacco smoke–induced emphysema by upregulating antioxidant defenses and decreasing lung inflammation and alveolar cell apoptosis.

Introduction

Pulmonary emphysema is a major manifestation of chronic obstructive pulmonary disease (COPD), which affects more than 16 million Americans and is the fourth highest cause of death in United States (1). COPD is the only disease among the top 10 causes of death with rising incidence in the United States, and it is predicted to reach worldwide epidemic proportions (2). Cigarette smoking accounts for most of this debilitating disease, but other environmental risk factors include air pollution and chronic occupational exposure to various dusts (3).

Permanent destruction of peripheral air spaces distal to terminal bronchioles is the hallmark of emphysema (4). Emphysema is also characterized by accumulation of inflammatory cells such as macrophages and neutrophils (1) in bronchioles and alveolar structures. In humans, a deficiency in antiproteinase inhibitors produced by inflammatory cells, such as α1-antitrypsin, has been shown to contribute to a protease/antiprotease imbalance, thereby favoring destruction of alveolar extracellular matrix in cigarette smoke–induced (CS-induced) emphysema (5, 6). MMPs play a central role in experimental emphysema, as documented by the resistance of macrophage metalloelastase knockout mice against emphysema caused by chronic inhalation of CS (7). Moreover, pulmonary overexpression of interleukin-13 in transgenic mice results in MMP- and cathepsin-dependent emphysema (8). There is recent evidence that apoptosis of alveolar septal cells also contributes to human emphysema and is required for experimental emphysema caused by inhibition of the vascular endothelial growth factor receptor (4).

Markers of oxidative stress (e.g., hydrogen peroxide and the end products of lipid peroxidation such as ethane, pentane, and 8-isoprostane) are elevated in the breath and serum of patients with COPD (9). Oxidative stress enhances inflammation, inactivates critical antiproteinase inhibitors such as α1-antitrypsin (10), and enhances apoptosis of alveolar cells (4). Inflammatory mediators such as interleukin-8 and tumor necrosis factor-α, which are increased in bronchoalveolar samples obtained from patients with COPD (10, 11), are regulated by proinflammatory redox-sensitive transcription factors, including nuclear factor-κB and activator protein-1. Numerous studies have demonstrated that the susceptibility of the lung to oxidative injury depends largely on the upregulation of protective antioxidant systems (10). Although oxidative stress, which originates from CS and infiltrating inflammatory cells, is suspected to be involved in the etiopathogenesis of

Nonstandard abbreviations used: ARE, antioxidant response element; BAL, bronchoalveolar lavage; COPD, chronic obstructive pulmonary disease; CS, cigarette smoke; EMSA, electrophoretic mobility shift assay; G6PDH, glucose-6-phosphate dehydrogenase; γ-GCS, γ-glutamyl cysteine synthase; GPx, glutathione peroxidase; GSR, glutathione reductase; GST, glutathione S-transferase; HO-1, heme oxygenase-1; NQO1, NADPH: quinone oxidoreductase-1; Nrf2, nuclear factor, erythroid-derived 2, like 2; OCT1, octamer transcription factor 1; 8-oxo-dG, 8-oxo-7,8-dihydro-2′-deoxyguanosine; Prx-1, peroxiredoxin-1; SpC, surfactant protein C; TrxR, thioredoxin reductase; TSS, transcription start site; UGT, UDP-glucuronosyl transferase.

Conflict of interest: The authors have declared that no conflict of interest exists.

Citation for this article: *J. Clin. Invest.* **114**:1248–1259 (2004). doi:10.1172/JCI200421146.

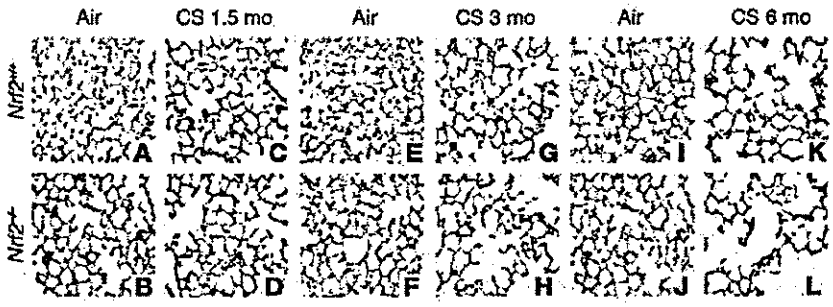

Figure 1
Increased susceptibility of *Nrf2*$^{-/-}$ mice to CS-induced emphysema. Shown are H&E-stained lung sections from *Nrf2*$^{+/+}$ and *Nrf2*$^{-/-}$ mice exposed to air alone (A and B, E and F, and I and J) and to CS (C and D, G and H, and K and L) at the indicated times. Sections from the air-exposed *Nrf2*$^{+/+}$ and *Nrf2*$^{-/-}$ mice show normal alveolar structure (n = 5 per group). Lung sections from the CS-treated (6 months) *Nrf2*$^{-/-}$ mice show increased air space enlargement when compared with the lung sections from the CS-treated *Nrf2*$^{+/+}$ mice. Original magnification, ×20.

the disease (10), there is no conclusive experimental evidence that supports a central role for oxidative stress in pathogenesis of CS-induced emphysema. Critical host factors that protect the lungs against oxidative stress may either directly determine susceptibility to alveolar tissue destruction in emphysema or act as modifiers of risk by affecting the intensity of inflammation associated with chronic CS inhalation.

Linkage analysis of hyperoxia-resistant and -sensitive mouse strains have identified *nuclear factor, erythroid-derived 2, like 2* (*Nrf2*) as a candidate gene for resistance to hyperoxic injury (12). *Nrf2* encodes a basic leucine zipper protein (bZIP) transcription factor which, upon activation in response to oxidative or electrophilic stress, detaches from its cytosolic inhibitor, Keap1, translocates to the nucleus, and binds to the antioxidant response element (ARE) in the promoter of target genes, leading to their transcriptional induction (13). Though little is known about Nrf2-regulated genes in the lungs, the recognized members of this group include several critical antioxidant genes, such as heme oxygenase-1 (HO-1), γ-glutamyl cysteine synthase (γ-GCS), and several members of the glutathione S-transferase (GST) family (13).

We have postulated that Nrf2 is a critical transcription factor that determines susceptibility to lung inflammation, oxidative stress, and alveolar cell apoptosis caused by chronic exposure to CS. In the present study, we demonstrate that disruption of the *Nrf2* gene led to earlier-onset and more extensive CS-induced emphysema in mice. Thus, responsiveness of the Nrf2 pathway in lung cells plays a critical role in attenuating the development of CS-induced emphysema.

Results

Histological and lung morphometric studies. Lungs from air-exposed *Nrf2*-disrupted (*Nrf2*$^{-/-}$) and wild-type (*Nrf2*$^{+/+}$) mice showed normal alveolar structure (Figure 1). Since the alveolar diameter of air-exposed *Nrf2*$^{-/-}$ mice was slightly smaller than that of air-exposed wild-type mice (Table 1), we undertook detailed lung morphometric measurements, as well as light microscopic and ultrastructural studies, to ensure that *Nrf2*$^{-/-}$ lung does not have delayed development or compromised structural integrity when maintained in normal room air. There were no significant differences in alveolar diameter and mean linear intercept between *Nrf2*$^{+/+}$ and *Nrf2*$^{-/-}$ lungs at 3 days, 10 days, 2 months, or 6 months of age (Supplemental Figure 1, A–C; supplemental material available at http://www.jci.org/cgi/content/full/114/1248/9/DC1). Histochemical staining for reticulin and elastin showed similar alveolar architecture in the wild-type and knockout lungs, with progressive attenuation of alveolar septa occurring between day 10 and 2 months of age in both genetic backgrounds (Supplemental Figure 1A). At 2 months of age, there was no significant difference in the total lung capacity (Supplemental Methods) between the air-exposed *Nrf2*$^{+/+}$ (1.19 ± 0.16 ml; average weight of mice, 23 ± 1.4 g) and *Nrf2*$^{-/-}$ mice (1.12 ± 0.19 ml; average weight of mice, 23 ± 1.2 g), and the proliferation rate was similar in *Nrf2*$^{+/+}$ and *Nrf2*$^{-/-}$ lungs (Supplemental Figure 1D). Finally, *Nrf2*$^{+/+}$ and *Nrf2*$^{-/-}$ lungs had similar ultrastructural alveolar organization, with alveolar-capillary membranes lined by type I epithelial cells, and both had normal alveolar type II cell populations (Supplemental Figure 2, A and B). Histological examination of the lung sections did not reveal any tumors in air- or CS-exposed mice. Furthermore, H&E-stained lung sections did not show any significant inflammation in the lungs of air-exposed *Nrf2*$^{+/+}$ or *Nrf2*$^{-/-}$ mice (Figure 1 and Supplemental Figure 1A).

To determine the role of Nrf2 in susceptibility to CS-induced emphysema, *Nrf2*-disrupted and wild-type *Nrf2* (ICR strain) mice were exposed to CS for 1.5 to 6 months, and CS-induced lung damage was assessed by computer-assisted morphometry. There was a dramatic increase in alveolar destruction in the lungs of *Nrf2*-disrupted mice when compared to wild-type ICR mice after 6 months of exposure to CS. Both the alveolar diameter (increased by 33.1% in *Nrf2*$^{-/-}$ vs. 8.5% in *Nrf2*$^{+/+}$ mice) and mean linear intercept (increased by 26.1% in *Nrf2*$^{-/-}$ vs. 8.3% in *Nrf2*$^{+/+}$ mice) were significantly higher in CS-exposed *Nrf2*-disrupted mice (Table 1 and Figure 1). Alveolar enlargement was detected in the lungs of *Nrf2*$^{-/-}$ mice as early as 3 months after exposure to CS began (Table 1 and Figure 1), suggesting an earlier onset of emphysema in *Nrf2*-disrupted mice. Long-term (6 months) exposure of *Nrf2*$^{+/+}$ mice to CS resulted in an increase of less than 10% in the mean linear intercept and alveolar

Table 1
Effect of chronic exposure to CS on lung morphometry

Groups	Time of exposure (mo)	Alveolar diameter (μm)			Mean linear intercept (μm)		
		Air	CS	% Increase	Air	CS	% Increase
Nrf2$^{+/+}$	1.5	37.2 ± 1.3	39.1 ± 1.5	5.1	51.9 ± 2.3	52.3 ±1.8	1.9
	3	37.5 ± 1.6	40.5 ± 1.4	7.9	51.8 ± 2.7	53.6 ± 1.6	3.3
	6	38.9 ± 1.5	42.2 ± 1.7	8.5	52.6 ± 2.1	57.0 ± 1.5	8.3
Nrf2$^{-/-}$	1.5	34.5 ± 1.3	37.0 ± 1.6	7.2	50.0 ± 2.0	52.1 ± 2.0	4.3
	3	34.9 ± 1.2	41.8 ± 1.4	19.5	52.1 ± 1.8	58.0 ± 2.1	11.2
	6	35.8 ± 1.4	47.7 ± 1.5^{A}	33.1	53.5 ± 1.7	67.5 ± 2.3^{A}	26.1

Values shown are the mean ± SEM for groups of 5 mice each. $^{A}P \leq 0.05$, significantly greater than the CS-exposed (6 months) *Nrf2*$^{+/+}$ mice.

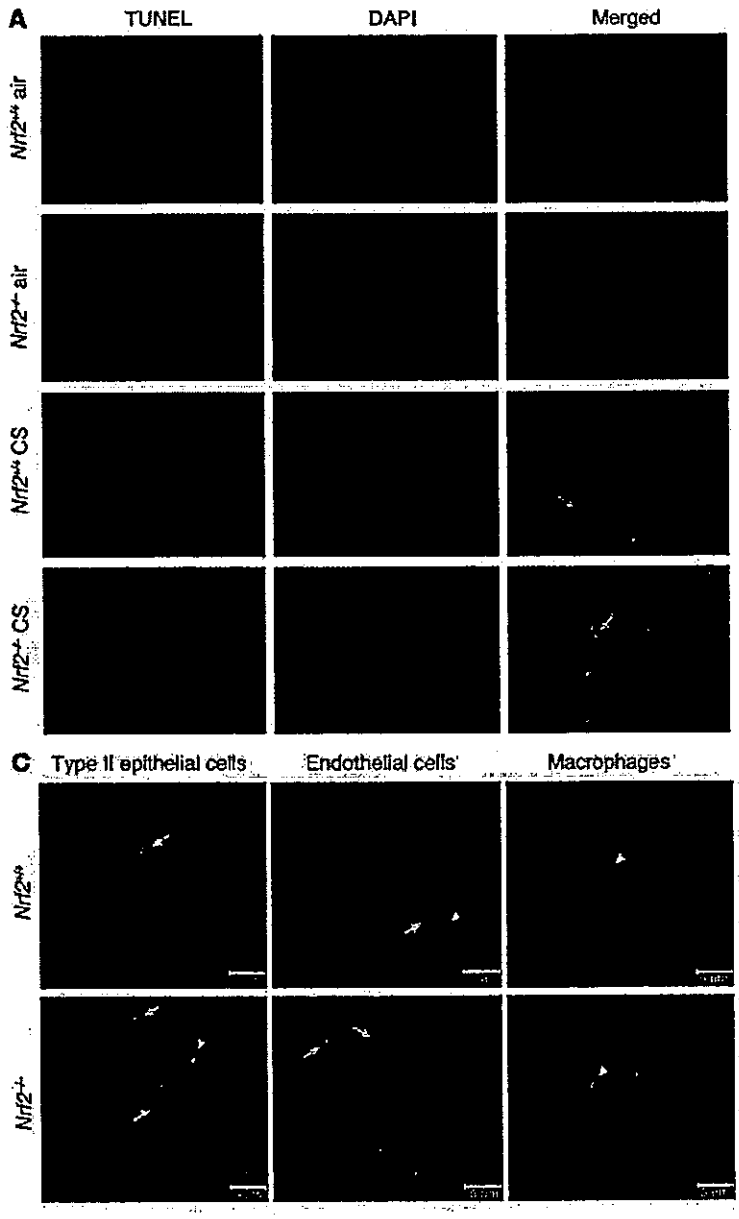

Figure 2
Cigarette smoke exposure causes lung cell apoptosis as assessed by TUNEL in *Nrf2*$^{-/-}$ lungs. (**A**) Lung sections (n = 5 per group) of room air– or CS-exposed (6 months) *Nrf2*$^{+/+}$ or *Nrf2*$^{-/-}$ mice were subjected to TUNEL (left column) and DAPI stain (middle column). Merged images are shown in the right column. CS-exposed *Nrf2*$^{-/-}$ mice show abundant TUNEL-positive cells (arrows) in the alveolar septa. Magnification, ×20. (**B**) Quantification of TUNEL-positive cells (per 1,000 DAPI-stained cells). The number of TUNEL-positive cells was significantly higher in the CS-exposed *Nrf2*$^{-/-}$ mice as compared with their wild-type counterparts (*$P \leq 0.05$). Values represent mean ± SEM. (**C**) Identification of apoptotic (TUNEL-positive) type II epithelial cells (left column), endothelial cells (middle column), and alveolar macrophages (right column) in the lungs of CS-exposed (6 months) *Nrf2*$^{+/+}$ and *Nrf2*$^{-/-}$ mice. Type II epithelial cells, endothelial cells, and alveolar macrophages were detected with anti-SpC, anti-CD34, and anti–Mac-3 antibodies, respectively, as outlined in Methods. Nuclei were detected with DAPI (blue). Shown are the merged images, with colocalization (yellow arrows) of cell-specific markers (cytoplasmic red signal) and apoptosis (nuclear green + blue DAPI signal, resulting in a lavender-like signal); non-apoptotic (TUNEL-negative) cells with positive cell specific marker (red signal) are highlighted with a red arrow. TUNEL-positive apoptotic cells lacking a cell-specific marker are highlighted by white arrowheads. The majority of TUNEL-positive cells consisted of endothelial and type II epithelial cells, whereas most alveolar macrophages were TUNEL negative. Scale bars: 5 μm.

diameter (Table 1), highlighting the intrinsic resistance of *Nrf2*$^{+/+}$ ICR mice to CS-induced pulmonary emphysema.

Apoptosis assays. To determine whether chronic exposure to CS (6 months) induced apoptosis of alveolar septal cells in vivo, we conducted TUNEL on lung sections from air- and CS-exposed mice. Labeling of DNA strand breaks in situ by fluorescent TUNEL demonstrated a higher number of TUNEL-positive cells in the alveolar septa of CS-exposed *Nrf2*$^{-/-}$ mice (154.27 TUNEL-positive cells per 1,000 DAPI-positive cells) than in CS-exposed *Nrf2*$^{+/+}$ mice (26.42 TUNEL-positive cells per 1,000 DAPI-positive cells) or in air-exposed *Nrf2*$^{-/-}$ or *Nrf2*$^{+/+}$ mice (Figure 2, A and B). Double staining of the TUNEL-labeled lung sections (Figure 2C) with antibody to surfactant protein C (SpC) to label type II epithelial cells, anti-CD34 to label endothelial cells, and anti–Mac-3 to label macrophages revealed the occurrence of apoptosis, predominantly in endothelial (*Nrf2*$^{-/-}$ = 52 ± 3.6 vs. *Nrf2*$^{+/+}$ = 8 ± 1.8 TUNEL-positive and CD34-positive cells per 1,000 DAPI-positive alveolar cells) and type II epithelial cells (*Nrf2*$^{-/-}$ = 43 ± 4.3 vs. *Nrf2*$^{+/+}$ = 6 ± 0.96 TUNEL-positive and SpC-positive cells per 1,000 DAPI-positive alveolar cells) in the lungs of CS-exposed *Nrf2*$^{-/-}$ mice when compared with *Nrf2*$^{+/+}$ mice. Most alveolar macrophages in CS-exposed lungs did not show evidence of apoptosis (*Nrf2*$^{-/-}$ = 5 ± 0.42 Mac-3–positive cells per 1,000 DAPI-positive cells vs. *Nrf2*$^{+/+}$ = 3 ± 0.96 Mac-3–positive cells per 1,000 DAPI-positive cells).

Immunohistochemical analysis showed a higher number of caspase-3-positive cells in the alveolar septa of CS-exposed *Nrf2*$^{-/-}$ mice (4.83 active caspase-3-positive cells/mm alveolar length) than in CS-exposed *Nrf2*$^{+/+}$ mice (1.09 active caspase-3–positive cells/mm alveolar length). Lung sections from the air-exposed control *Nrf2*$^{-/-}$ and wild-type mice showed few or no caspase-3–posi-

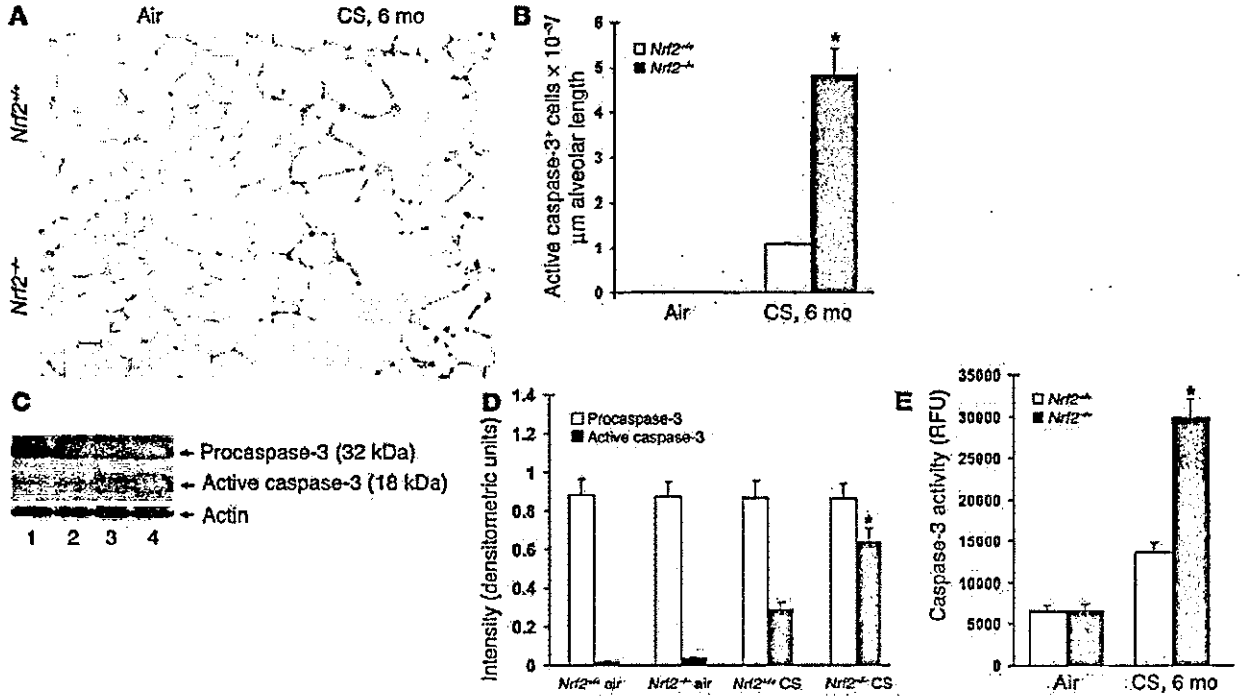

Figure 3

CS treatment leads to activation of caspase-3 in *Nrf2*$^{-/-}$ lungs. (A) Active caspase-3 expression in lung sections from CS-exposed (6 months) *Nrf2*$^{+/+}$ and *Nrf2*$^{-/-}$ mice. CS-exposed *Nrf2* $^{-/-}$ mice show increased numbers of caspase-3–positive cells in the alveolar septa ($n = 5$ per group). Magnification, ×40. (B) Number of caspase-3–positive cells in the lungs of air- and CS-exposed mice. Caspase-3–positive cells were significantly higher in the lungs of CS-exposed *Nrf2*$^{-/-}$ mice. (C) Increased expression of the 18-kDa active form of caspase-3 in lungs of CS-exposed (6 months) *Nrf2*$^{-/-}$ mice (Western blot; lanes 1 and 3: air- and CS-exposed *Nrf2*$^{+/+}$ mice, respectively; lanes 2 and 4: air- and CS-exposed *Nrf2*$^{-/-}$ mice, respectively). (D) Quantification of procaspase-3 and active caspase-3 obtained in Western blots of air- or CS-exposed *Nrf2*$^{+/+}$ and *Nrf2*$^{-/-}$ lungs. Values are represented as mean ± SEM. (E) Caspase-3 activity in the lungs of air- or CS-exposed (6 months) *Nrf2*$^{+/+}$ and *Nrf2*$^{-/-}$ mice. Caspase-3 activity was significantly higher in the lungs of CS-exposed *Nrf2*$^{-/-}$ mice than in the lungs of their wild-type counterparts ($n = 3$ per group). Values (relative fluorescence units [RFU]) are represented as mean ± SEM. *$P \leq 0.05$ vs. CS-exposed *Nrf2*$^{+/+}$ mice.

tive cells (Figure 3, A and B). Enhanced activation of caspase-3 in *Nrf2*$^{-/-}$ lungs exposed to CS for 6 months was further documented by the increased detection of the 18-kDa active caspase-3 peptide in whole-lung lysates (increase in *Nrf2*$^{-/-}$ mice was 2.3-fold that of CS-exposed *Nrf2*$^{+/+}$ mice; Figure 3, C and D), as well as by increased caspase-3 enzymatic activity (increase in activity in *Nrf2*$^{-/-}$ mice was 2.1-fold that of CS-exposed *Nrf2*$^{+/+}$ mice; Figure 3E).

Marker of oxidative stress in the lungs. Immunohistochemical staining with anti-8-oxo-7,8-dihydro-2′-deoxyguanosine (anti-8-oxo-dG) antibody was used to assess oxidative stress in both *Nrf2*$^{-/-}$ and *Nrf2*$^{+/+}$ lungs after inhalation of CS. A small number of alveolar septal cells (1.78 cells/mm alveolar length) exhibited staining for 8-oxo-dG in lung sections from the *Nrf2*$^{+/+}$ mice, whereas significantly more (16.8 cells/mm alveolar length) were stained in the *Nrf2*$^{-/-}$ mice (Figure 4, A and B). Lung sections from air-exposed *Nrf2*$^{+/+}$ and *Nrf2*$^{-/-}$ mice showed few or no 8-oxo-dG–positive cells. Immunostaining with normal mouse IgG antibody did not show any IgG-reactive cells in the lungs of air- or CS-exposed mice (Figure 4C). These results indicate that exposure to CS for 6 months enhanced oxidative damage to the lungs of the *Nrf2*-disrupted mice.

Inflammatory cells in the lungs. Analysis of differential cell counts in the bronchoalveolar lavage (BAL) fluid revealed a significant increase in the number of total inflammatory cells in the lungs of CS-exposed (1.5 or 6 months) *Nrf2*$^{+/+}$ and *Nrf2*$^{-/-}$ mice when compared to their respective air-exposed control littermates (Figure 5A). However, the total number of inflammatory cells in BAL fluid from the CS-exposed *Nrf2*$^{-/-}$ mice was significantly higher than in CS-exposed wild-type mice. Among the inflammatory cell population, macrophages were the predominant cell type, constituting as much as 87–90% of the total inflammatory cell population in the BAL fluid of both genotypes exposed to CS. Other inflammatory cells such as polymorphonuclear leukocytes, eosinophils, and lymphocytes constituted 10–13% of the total inflammatory cells in the BAL fluid of both genotypes. Immunohistochemical staining of the lung sections with Mac-3 antibody revealed the presence of an increased number of macrophages (Figure 5, B and C) in the lungs of CS-exposed *Nrf2*$^{-/-}$ mice at 6 months (4.54 Mac-3–positive cells/mm alveolar length) when compared with lungs of their wild-type counterparts (2.27 Mac-3–positive cells/mm alveolar length). However, the immunohistochemical staining did not show any significant difference in the number of alveolar macrophages in the lungs of air-exposed *Nrf2*$^{+/+}$ (0.96 Mac-3–positive cells/mm alveolar length) and *Nrf2*$^{-/-}$ mice (1.18 Mac-3–positive cells/mm alveolar length). There were significantly fewer neutrophils and lymphocytes than there were macrophages. There were 0.92 versus 0.49 neutrophils and 0.78 versus 0.43 lymphocytes per millimeter alveolar length in CS-exposed *Nrf2*$^{-/-}$ and wild-type mice, respectively (Supplemental Figure 3, A–D).

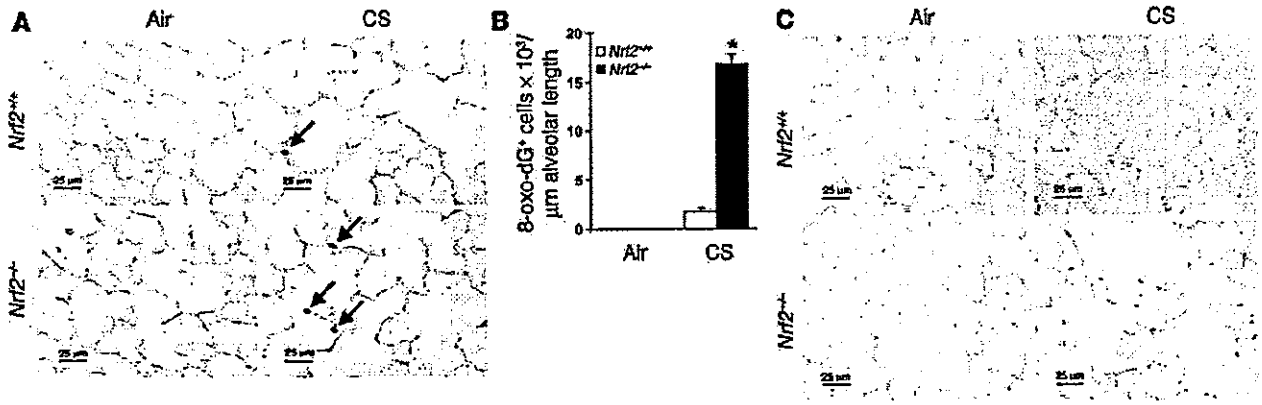

Figure 4
Increased sensitivity of *Nrf2*$^{-/-}$ mice to oxidative stress after CS exposure. (**A**) Immunohistochemical staining for 8-oxo-dG in lung sections from the mice exposed to CS (6 months) (n = 5 per group). Lung sections from the CS-exposed *Nrf2*$^{-/-}$ mice show increased staining for 8-oxo-dG (indicated by arrows) when compared with lung sections from CS-exposed *Nrf2*$^{+/+}$ mice and the respective air-exposed control mice. Magnification, ×40. (**B**) Quantification of 8-oxo-dG–positive alveolar septal cells in lungs after 6 months of CS exposure. The number of cells that reacted with anti–8-oxo-dG antibody was significantly higher in the lung tissues of the CS-exposed *Nrf2*$^{-/-}$ mice than in the lung tissues of the CS-exposed *Nrf2*$^{+/+}$ mice and air-exposed control mice. Values (positive cells/mm alveolar length) represent mean ± SEM. *$P \leq 0.05$ vs. CS-exposed *Nrf2*$^{+/+}$ mice. (**C**) Immunohistochemical staining with normal mouse-IgG1 antibody in lung sections from air- or CS-exposed *Nrf2*$^{+/+}$ and *Nrf2*$^{-/-}$ mice. Magnification, ×40. Scale bars: 25 µm.

Activation of Nrf2 in the lungs of Nrf2$^{+/+}$ *mice.* An electrophoretic mobility shift assay (EMSA) was used to determine the activation and DNA binding activity of Nrf2 in the lungs in response to acute exposure of the mice to CS (5 hours). In response to CS, there was an increased binding of nuclear proteins isolated from the lungs of CS-exposed *Nrf2*$^{+/+}$ mice to an oligonucleotide probe containing the ARE consensus sequence, as compared to the binding of nuclear proteins isolated from CS-exposed *Nrf2*$^{-/-}$ mice or air-exposed control mice. Supershift analysis with anti-Nrf2 antibody also showed the binding of Nrf2 to the ARE consensus sequence, suggesting the activation of Nrf2 in the lungs of *Nrf2*$^{+/+}$ mice in response to CS exposure (Figure 6A). However, supershift analysis of the nuclear proteins from the lungs of CS-exposed *Nrf2*$^{-/-}$ mice with anti-Nrf2 antibody did not show any super-shifted band, consistent with the absence of Nrf2 in the ARE-nuclear protein complex.

Western blot analysis was performed to determine the nuclear accumulation of Nrf2 in the lungs in response to CS exposure. Immunoblot analysis (Figure 6B) showed increased levels of Nrf2 in the nuclei isolated from the lungs of CS-exposed *Nrf2*$^{+/+}$ mice, suggesting the nuclear accumulation of Nrf2 in the lungs of wild-type mice in response to CS exposure. Increase of nuclear Nrf2 is needed for the activation of ARE and the transcriptional induction of various antioxidant genes.

Transcriptional induction of Nrf2-dependent genes. To uncover the Nrf2-dependent genes that may account for the emphysema-sensitive phenotype of the *Nrf2*$^{-/-}$ background, we examined the pulmonary expression profile of air- and CS-exposed (5 hours) mice by oligonucleotide microarray analysis using the Affymetrix mouse gene chip U74A. The complete gene expression data set is available at http://faculty.jhsph.edu/biswal2.xls. Table 2 lists the genes that were significantly upregulated in the lungs of *Nrf2*$^{+/+}$ mice, but not in those of *Nrf2*$^{-/-}$ mice, in response to CS. The regions upstream of the transcription start site of these Nrf2-dependent genes were analyzed for the presence of putative AREs using the Genamics Expression 1.1 Pattern Finder Tool software. The location of the AREs in these Nrf2-dependent genes are also presented in Table 2. Nrf2 regulates about 50 antioxidant and cytoprotective genes. The majority of these Nrf2-regulated genes contain possible functional AREs in the genomic sequences upstream of their transcription start sites.

Validation of microarray data by Northern blot and enzyme assay. Validation of the microarray data was performed using the samples used in the arrays. Northern hybridization confirmed the transcriptional induction of genes involved in glutathione synthesis (glutamate cysteine ligase modifier subunit [GCLm]), NADPH regeneration (glucose-6-phosphate dehydrogenase [G6PDH]), detoxification of oxidative stress–inducing components of CS (by NADPH: quinone oxidoreductase-1 [NQO1], GST-α1, HO-1, thioredoxin reductase [TrxR], and peroxiredoxin-1 [Prx-1]) in the lungs of CS-exposed *Nrf2*$^{+/+}$ but not *Nrf2*$^{-/-}$ mice (Figure 7A). Glutathione reductase (GSR) was also induced in CS-exposed *Nrf2*$^{-/-}$ mice; however, the magnitude of the induction was significantly higher in *Nrf2* wild-type mice than in *Nrf2*-disrupted mice. The increases in these induced genes (NQO1, 7.2-fold; GST-α1, 2-fold; heavy subunit of γ-GCS [γ-GCS(h)], 4.8-fold; TrxR, 4.8-fold; G6PDH, 2.2-fold; HO-1, 3.4-fold; GSR, 1.8 fold; Prx-1, 1.6-fold), as measured by Northern analysis, were comparable to those determined by microarray.

Enzyme assays of selected gene products (NQO1, GSR, Prx, glutathione peroxidase [GPx] and G6PDH) were carried out to determine the extent to which their transcriptional induction in the lung paralleled changes in their activities (Figure 7B). There were significant increases in the activities of all enzymes in the lungs of CS-exposed *Nrf2*$^{+/+}$ mice when compared to those of CS-exposed *Nrf2*$^{-/-}$ mice as well as those of the air-exposed mice of both genotypes. Moreover, the basal activities of these enzymes were significantly lower in the air-exposed *Nrf2*-disrupted mice than in the air-exposed wild-type mice.

Discussion

Our findings indicate that Nrf2, as previously shown for MMP-12, is a critical determinant of susceptibility to emphysema caused by CS. Because oxidative stress has overarching effects on several impor-

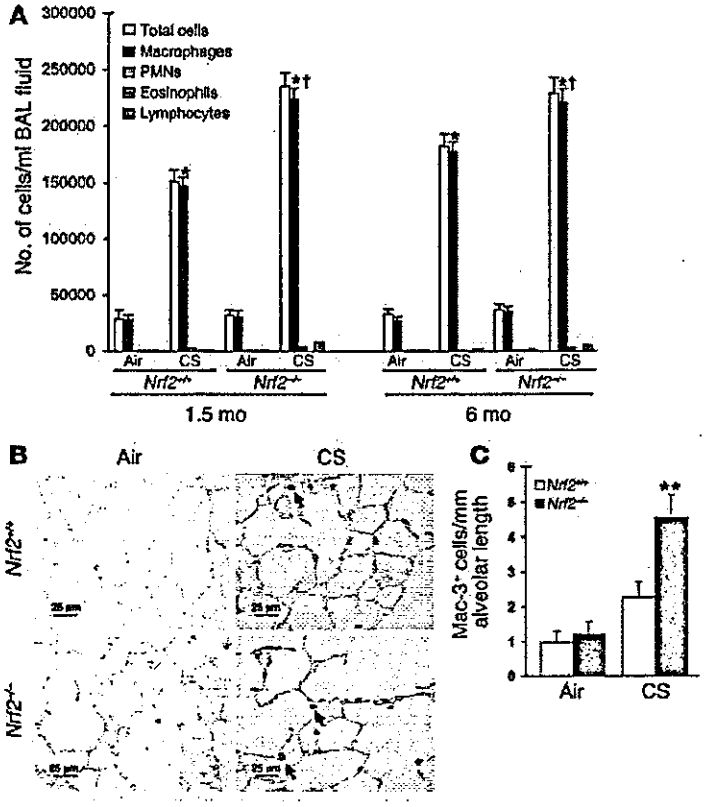

Figure 5
Increased inflammation in the lungs of CS-exposed *Nrf2*$^{-/-}$ mice. (**A**) Lavaged inflammatory cells from control and CS-exposed mice. The number of macrophages in BAL fluid collected from the CS-exposed (both 1.5 months and 6 months) *Nrf2*$^{-/-}$ mice was significantly higher than in the BAL fluid from CS-exposed *Nrf2*$^{+/+}$ mice and the respective age-matched control mice. Values represent mean ± SEM ($n = 8$). PMNs, polymorphonuclear leukocytes. $^{*}P \leq 0.05$ vs. control of the same genotype; $^{\dagger}P \leq 0.05$ across the genotypes in CS-exposed group. (**B**) Immunohistochemical detection of macrophages (arrows) in lungs of *Nrf2*$^{+/+}$ and *Nrf2*$^{-/-}$ mice exposed to CS for 6 months. Magnification, ×40. Scale bars: 25 μm. (**C**) Quantification of macrophages in lungs after 6 months of CS exposure. The lung sections from the CS-exposed *Nrf2*$^{-/-}$ mice showed significantly more macrophages than did those from wild-type counterparts exposed to CS ($^{**}P \leq 0.025$). However, there was no significant difference in the number of alveolar macrophages between the air-exposed *Nrf2*$^{+/+}$ and *Nrf2*$^{-/-}$ mice ($P > 0.9$).

tant mechanisms involved in CS-induced emphysema, particularly inflammation and apoptosis, Nrf2-induced gene expression may afford wide protection against the injurious effects of CS in the lung. The enhanced susceptibility of *Nrf2*-disrupted mice to CS-induced emphysema is remarkable, since the ICR parental strain (14) has been shown to be intrinsically resistant to CS-induced alveolar destruction and air space enlargement, as compared to susceptible strains such as C57BL/6J and DBA/2 (15). The higher levels of antioxidants and α1-antitrypsin in the lungs of ICR strain mice, as compared to those of susceptible strains, may contribute to this resistance (15).

We found that deletion of *Nrf2* resulted in increased alveolar inflammation, alveolar septal cell apoptosis involving predominantly endothelial and type II epithelial cells, enhanced alveolar oxidative stress, and ultimately more pronounced emphysema following exposure to CS, when compared with wild-type mice. Such broad lung pathogenic effects resulting from elimination of *Nrf2* indicate that, in CS-induced emphysema, oxidative stress regulates the intensity of alveolar inflammation, the extent of alveolar cell ap-optosis, and ultimately the rate of onset and severity of the emphysema. In fact, the increased severity of CS-induced emphysema caused by deletion of *Nrf2* in ICR mice is equivalent to that seen in MMP-12-competent C57Bl/6J mice (when compared to MMP12$^{-/-}$ mice) (7). Despite abundant evidence of the elevation of markers of pulmonary and systemic oxidative stress in chronic smokers, there is a paucity of mechanistic support for the centrality of oxidative stress in the pathogenesis

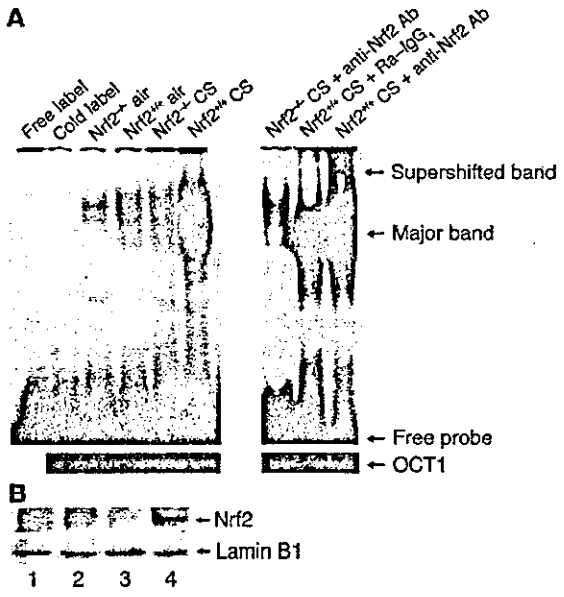

Figure 6
Activation of Nrf2 in CS-exposed *Nrf2*$^{+/+}$ lungs. (**A**) EMSA to determine the DNA binding activity of Nrf2. For gel shift analysis, 10 μg of nuclear protein from the lungs of air-and CS-exposed mice was incubated with the labeled human NQO1 ARE sequence and analyzed on a 5% non-denaturing polyacrylamide gel. For supershift assays, the labeled NQO1 ARE was first incubated with 10 μg of nuclear extract and then with 4 μg of anti-Nrf2 antibody for 2 hours. Nuclear protein of *Nrf2*$^{+/+}$ lungs showed increased binding to the ARE-containing sequence (lower arrow) after CS exposure, with a supershifted band caused by preincubation with anti-Nrf2 antibody, thus confirming the binding of Nrf2 to the ARE sequence (upper arrow). Ra–IgG$_1$, rabbit IgG$_1$. (**B**) Nuclear accumulation of Nrf2. Western blot analysis with anti-Nrf2 antibody showed the nuclear accumulation of the transcription factor Nrf2 in the lungs of *Nrf2*$^{+/+}$ mice in response to CS exposure (lanes 1 and 3: air-exposed *Nrf2*$^{-/-}$ and *Nrf2*$^{+/+}$ mice, respectively; lanes 2 and 4: CS-exposed *Nrf2*$^{-/-}$ and *Nrf2*$^{+/+}$ mice, respectively; lamin B1 was used as the loading control). Western blot analysis was carried out 3 times with the nuclear proteins isolated from the lungs of 3 different air- or CS-exposed *Nrf2*$^{+/+}$ and *Nrf2*$^{-/-}$ mice.

Table 2
Nrf2-dependent protective genes induced by CS in the lungs of *Nrf2* wild-type mice

Functional classification and gene accession no.	Gene	Fold change ± SE	ARE position
Antioxidants			
X56824 (X06985)	*Heme oxygenase 1*[A]	4.7 ± 0.4	–3928, –3992, –6007, –7103, –8978, –9007, –9036, –9065, –9500
U38261 (U10116)	*Superoxide dismutase 3*[B]	1.7 ± 0.4	–2362, –3171, –5282
X91864 (X68314)	*Glutathione peroxidase 2*[B]	2.7 ± 0.4	–44, –3600
U13705 (X58295)	*Glutathione peroxidase 3*[B]	1.4 ± 0.4	–7144, –9421
U85414 (M90656)	*Gamma glutamylcysteine synthase (catalytic)*[A]	7.6 ± 0.5	–3479, –3524, –5421
U95053 (L35546)	Gamma glutamylcysteine synthase (regulatory)[A]	7.3 ± 0.5	–44
AF090686 (M60396)	*Transcobalamine II*[B]	1.6 ± 0.3	–3751, –6382, –8236
L39879 (BC004245)	*Ferritin light chain 1*[A]	1.5 ± 0.3	–1379
AI118194 (X67951)	*Peroxiredoxin 1*[B]	1.5 ± 0.3	–78, –8413, –9652
AI851983 (X15722)	*Glutathione reductase*[B]	3.3 ± 0.4	–115, –9433
AB027565 (X91247)	*Thioredoxin reductase 1*[B]	4.3 ± 0.4	–121, –4326, –9521
Z11911 (X03674)	*Glucose-6-phosphate dehydrogenase*[B]	2.0 ± 0.3	–2504, –2109
AW120625 (U30255)	*Phosphogluconate dehydrogenase*[B]	2.1 ± 0.4	–757, –3963
Detoxification enzymes			
L06047(AF025887)	*Glutathione-S-transferase, α1*[B]	2.0 ± 0.3	NF
J03958 (M16594)	*Glutathione-S-transferase, α2*[A]	2.6 ± 0.3	–6662,– 6961, –7751
X65021	*Glutathione-S-transferase, α3*[B]	1.5 ± 0.3	No human homolog
AI843119 (U90313)	Glutathione-S-transferase, θ1[B]	2.0 ± 0.3	–255
X53451 (X06547)	Glutathione-S-transferase, π2[B]	3.1 ± 0.3	–71
J03952 (J03817)	*Glutathione-S-transferase GT8.7*[B]	1.6 ± 0.3	–1209
U12961 (J03934)	*NADPH: quinone reductase 1*[A]	9.3 ± 0.5	–527
U20257 (U09623)	Alcohol dehydrogenase 7 (class IV)[B]	2.8 ± 0.3	–2894
AV089850 (M74542)	Aldehyde dehydrogenase family 3, subfamily A1[B]	11.1 ± 0.8	–4223
U04204	*Aldo-keto reductase1, member B8*[B]	5.4 ± 0.5	No human homolog
AB017482 (AH005616)	*Retinol oxidase/Aldehyde oxidase*[B]	2.3 ± 0.4	–8579
AB025408 (AF112219)	*Esterase 10*[B]	3.4 ± 0.4	–4105, –4264
U16818 (J04093)	*UDP-glucuronosyl transferase*[B]	1.4 ± 0.3	–5431, –6221
AF061017 (AF061016)	*UDP-glucose dehydrogenase*[B]	1.5 ± 0.6	–3438
Protective proteins			
M64086 (AH002551)	*α1-antitrypsin proteinase inhibitor*[B]	4.7 ± 0.3	–4117
AB034693 (AB034695)	*Endomucin-1*[B]	1.5 ± 0.3	–2565
AW120711 (AF087870)	*Dnaj (HSP 40) homolog*[B]	1.9 ± 0.4	–155, –2797, –5320
D17666 (AU130219)	*Mitochondrial stress – 70 protein*[B]	1.6 ± 0.3	–2675, –3302
AF055638 (AF265659)	*GADD45G*[B]	2.4 ± 0.3	–327
U08210 (M16983)	*Tropoelastin*[B]	2.8 ± 0.9	NF
X04647 (X05562)	Procollagen type IV, α2[B]	1.9 ± 0.4	NF
Transcription factors			
AB009694 (AJ010857)	*mafF*[B]	2.6 ± 0.4	–3894, –6537, –8279, –8301, –8445
AF045160 (U81984)	*HIF-1α related factor*[B]	2.0 ± 0.4	–3855, –5091
Protein degradation			
AV305832 (M26880)	*Ubiquitin C*[B]	1.8 ± 0.4	–1393, –3755, –4481
AW121693 (AA020857)	Proteasome (prosome, macropain) 26S subunit, non ATPase, 1[B]	1.7 ± 0.3	NF
U40930 (BC017222)	*Sequestosome 1*[B]	2.9 ± 0.4	–360, –1328
Transporters			
M22998* (K03195)	*Solute carrier family 2*[B]	2.9 ± 0.2	–3351, –5111, –9304
X67056 (S70612)	*Glycine transporter*[B]	1.8 ± 0.3	–387, –8451
U75215 (BC026216)	*Neutral amino acid transporter mASCT1*[B]	3.8 ± 0.3	–3695, –8547
Phosphatases			
M97590 (AH003242)	*Tyrosine phosphatase (PTP1)*[B]	1.6 ± 0.3	–6045, –3232, –7029, –9884
X58289 (X5431)	Protein tyrosine phosphatase, receptor type B[B]	1.7 ± 0.4	–8166, –9561, –9662
Receptor			
AJ250490 (AJ001015)	*Receptor activity modifying protein 2*[B]	1.6 ± 0.3	–5023, –3455

AREs reported in the table are for human genes homologous to the respective mouse gene; the number in parenthesis refers to GenBank human accession number. To locate the AREs in each gene, we scanned 10-kb sequences upstream of the TSS in both strands using the ARE consensus sequence RTGAYNNNGCR as probe; the TSS for each gene was determined by following the Human Genome *build 34*, version 1 of the NCBI database. [A]Genes that have already been reported to have AREs and to be regulated by Nrf2; [B]Genes with the newly identified AREs using Genamics Expression 1.1 Pattern Finder Tool software (see Methods). NF, not found.

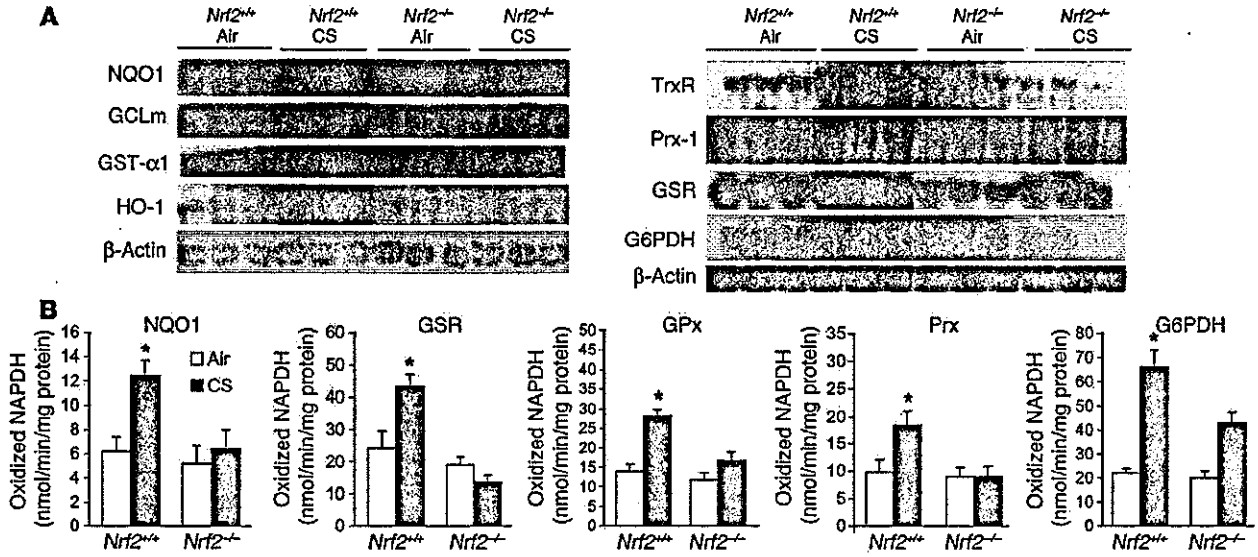

Figure 7

Validation of microarray data by Northern blot and enzyme assays. (A) Analysis of mRNA levels of NQO1, GCLm, GST-α1, HO-1, TrxR, Prx-1, GSR, and G6PDH in the lungs of *Nrf2*$^{+/+}$ and *Nrf2*$^{-/-}$ mice exposed to either air or CS ($n = 3$ per group). (B) Effect of CS on the specific activities of selected enzymes in the lungs of *Nrf2*$^{+/+}$ and *Nrf2*$^{-/-}$ mice. Values represent mean ± SE ($n = 3$ per group). *$P \leq 0.05$ vs. control of the same genotype.

of CS-induced emphysema. An oxidative burden in the smoker's lungs is generated by the 4,700 chemical components present in CS and by the inflammatory cells that accumulate in the smoker's airways. This oxidative burden elicits a protective response that is dependent upon the ability of the lung cells to upregulate antioxidant defenses. The upregulation and activation of transcription factors such as Nrf2 might be one of these protective mechanisms. Prior and concomitant to airspace enlargement caused by CS exposure, there was an increased infiltration of inflammatory cells, predominantly macrophages, which may have contributed to the alveolar injury through the activity of their elastolytic enzymes, particularly MMP-12 (7). A decrease in the activity and levels of antiproteases might have followed the enhanced oxidative stress in our model and thus contributed to protease/antiprotease imbalance. However, future studies will determine the role of specific proteases in the development of emphysema in *Nrf2*$^{-/-}$ mice in response to CS.

In addition to inflammation, the lungs of *Nrf2*-disrupted mice show increased alveolar cell apoptosis when compared to wild-type lungs. Alveolar cell apoptosis has been progressively recognized as a critically important mechanism of alveolar septal destruction in emphysema. Apoptosis is required for emphysema caused by VEGF receptor inhibition and is sufficient to cause emphysema, as demonstrated in mice instilled intrabronchially with active caspase-3 (16). However, the contribution of alveolar cell apoptosis has not been addressed in animal models of CS-induced emphysema. Long-term exposure to CS resulted in increased apoptosis of endothelial and type II epithelial cells at the 6-month time point in the lungs of CS-exposed *Nrf2*$^{-/-}$ mice when compared with CS-exposed *Nrf2*$^{+/+}$ mice. Staining of the TUNEL-labeled lung sections with Mac-3 antibody showed the presence of few or no apoptotic macrophages in the lungs of CS-exposed *Nrf2*$^{+/+}$ or *Nrf2*$^{-/-}$ mice. Immunohistochemical staining, enzyme assay, and Western blot analysis have also revealed the increased number or activity of caspase-3 in the lungs of CS-exposed *Nrf2*$^{-/-}$ mice, suggesting the occurrence of excessive apoptosis. The presence of enhanced lung apoptosis in these *Nrf2*$^{-/-}$ mouse lungs might be related to enhanced oxidative stress, inflammation, or excessive lung proteolysis. Oxidative stress and apoptosis are part of a mutually interactive feedback loop in VEGF receptor blockade-induced emphysema (4). Furthermore, reactive oxygen and nitrogen species can modify and inactivate survival cell signaling molecules and cause apoptosis. Inflammation and protease/antiprotease imbalance may also promote apoptosis by means of activated T lymphocytes, which are increased in COPD and seem to correlate with the degree of emphysema (17) and the amount of unopposed leukocyte elastase (18), gelatinase, or collagenase (19) activity.

Consistent with a central role for Nrf2 in the upregulation of antioxidant defenses during CS-related stress, in *Nrf2*$^{-/-}$ mice exposed to CS, there was an enhanced formation of 8-oxo-dG, one of the most abundant DNA adducts in response to oxidative stress (20). The importance of Nrf2 in affording protection during oxidative stress has already been highlighted by the enhanced susceptibility of *Nrf2*$^{-/-}$ mice to hyperoxia (12, 21) and chemically induced lung injury (22). The majority of the genes that were significantly upregulated in the lungs of CS-exposed *Nrf2* wild-type mice, but not *Nrf2*-disrupted mice, have functions likely to confer protection against oxidative stress and inflammation.

Nrf2 — in association with several other proteins such as small maf proteins, c-jun, ARE binding protein-1, CBP/p300, and p160 family coactivators — binds to ARE, leading to transcriptional induction of target genes (23, 24). In response to CS exposure, there was an increased binding of nuclear proteins from the lungs of *Nrf2*$^{+/+}$ mice to the ARE sequence. This binding is presumably due to the interaction of nuclear proteins with the ARE, particularly of Nrf2 in the lungs of CS-exposed *Nrf2*$^{+/+}$ mice, as confirmed by the supershift analysis with anti-Nrf2 antibody. The slightly increased binding of nuclear proteins to ARE in knockout lung

extracts is probably due to the involvement of proteins other than Nrf2, since the supershift analysis failed to detect a complex of Nrf2 in *Nrf2*$^{-/-}$ lung extracts. Western blot analysis confirmed the nuclear accumulation of Nrf2 in the lungs of CS-exposed *Nrf2*$^{+/+}$ mice. Increased nuclear Nrf2 is critical for the activation of ARE and the transcriptional induction of various antioxidant genes.

Nrf2, in response to CS, regulates genes involved in two major redox systems, the glutathione and thioredoxin systems (25, 26). Enzymes involved in glutathione synthesis (γ-GCS catalytic and regulatory subunits), members of the GST family, GSR, GPx2, GPx3, and genes that constitute the thioredoxin system (TrxR and Prx-1) were all induced in the lungs of *Nrf2*$^{+/+}$ mice in response to CS. The members of these redox systems interact with various transducers and effector molecules to bring about antioxidant-specific responses. The regeneration of reduced Trx and glutathione by TrxR and GSR, respectively, utilizes NADPH as a reducing equivalent generated by G6PDH and phosphogluconate dehydrogenase, both of which are also induced in *Nrf2*$^{+/+}$ lungs. Prx-1 and GPx reduce hydroperoxides by utilizing two electrons provided by Trx and glutathione, respectively. In addition, GPx and peroxiredoxins have been shown to play a potential role in protection against peroxynitrite (27), a potent oxidant generated from the reaction of superoxide and nitrous oxide present in CS. Furthermore, the oxidized forms of GPx and peroxiredoxins are reduced back to their functional forms by Trx (28). These results suggest a cross talk between the thioredoxin and glutathione redox systems and the NADPH regenerating system.

Several GSTs, as well as UDP-glucuronosyl transferase (UGT) and NQO1, were selectively induced only in *Nrf2*$^{+/+}$ mice in response to CS. Various isoforms of GSTs and UGTs play important roles in the detoxification of tobacco smoke carcinogens such as 4-(methylnitrosamino)-1-(3-pyridyl)-1-butanone, benzo(a)pyrene and other polycyclic aromatic hydrocarbons that act as electrophiles and cause DNA damage and cytotoxicity (29, 30). NQO1 blocks redox cycling of polyaromatic hydrocarbons and benzoquinones present in CS (31), thereby reducing the levels of ROS and presumably 8-oxo-dG. Various enzymes, including aldehyde dehydrogenase and aldo-keto reductase, which are involved in the detoxification of reactive aldehydes such as acetaldehyde and acrolein, were selectively induced in the lungs of CS-exposed *Nrf2*$^{+/+}$ mice. HO-1, a critical enzyme involved in protection against oxidant-mediated cellular injury, as well as the iron-sequestering protein ferritin light chain 1, which prevents uncontrolled surges in the intracellular free concentration of the highly reactive yet poorly soluble ferric iron (32, 33), were induced only in the lungs of CS-exposed *Nrf2*$^{+/+}$ mice. Reduction of ferric iron by superoxide can generate reactive hydroxyl radicals via the Fenton reaction. Superoxide dismutase 3, the major extracellular antioxidant enzyme in the lung that attenuates ROS-mediated lung cell injury and inflammation, is also selectively upregulated in *Nrf2*$^{+/+}$ mice in response to CS (34). CS also induced heat shock proteins such as HSP40 and mitochondrial stress-70 protein, as well as ubiquitin C, a protein involved in the degradation of oxidized proteins. Other Nrf2-regulated genes included the DNA damage repair protein GADD45G, lung structural proteins such as tropoelastin and procollagen type IV, α2, and endomucin-1, sequestosome 1, MafF, HIF-1α–related factor and α1-antitrypsin proteinase inhibitor. Mutations in the α1-antitrypsin proteinase inhibitor have been associated with an increased risk of COPD (35). Furthermore, we have located one or more AREs in the upstream regions of most of these differentially expressed genes, indicating the possibility of a direct role for Nrf2 in their transcriptional induction.

Taken together, these results provide a clear link between a defective response of the transcription factor Nrf2 and several lung problems: excessive oxidative stress, increased apoptosis, inflammation, and worsened emphysema. Nrf2 is activated in response to CS in the lungs of wild-type mice, leading to transcriptional induction of target genes that might provide resistance against the development of emphysema. Conversely, a lack of responsiveness of the Nrf2 pathway confers susceptibility to severe emphysema due to CS exposure in this model. The identification of Nrf2 as a determinant of susceptibility can have wide implications in the area of tobacco smoke–related lung diseases, where oxidative stress and inflammation play important roles.

Methods

Antibodies and reagents. We used the following antibodies and reagents: anti-caspase-3 polyclonal antibody for immunohistochemistry (Idun Pharmaceuticals); biotinylated anti-mouse IgG, peroxidase-conjugated streptavidin, Vectashield HardSet mounting medium, and RTU HRP-avidin complex (Vector Laboratories); rabbit anti-SpC antibody (Chemicon International Inc.); rat anti-mouse Mac-3 antibody (BD Biosciences); anti-rabbit Texas red antibody, streptavidin-Texas red conjugated complex, and DAPI (Molecular Probes Inc.); biotinylated rabbit anti-mouse secondary antibody (DakoCytomation); octamer transcription factor 1 (OCT1) and CaspACE Assay kit (Promega Corp.); leupeptin, pepstatin A, and normal mouse IgG_1 (Sigma-Aldrich); rat anti-mouse neutrophil antibody (Serotec); actin and anti-mouse CD45R primary antibody (Santa Cruz Biotechnology Inc.); rabbit anti-caspase-3 antibody for Western blot (Cell Signaling Technology Inc.); anti-CD34 and anti-lamin B1 antibody (Zymed Laboratories Inc.); and CH11 monoclonal antibody (Beckman Coulter Inc.).

Animals and care. *Nrf2*-deficient ICR mice were generated as described (14). Mice were genotyped for *Nrf2* status by PCR amplification of genomic DNA extracted from blood (36). PCR amplification was carried out using 3 different primers: 5′-TGGACGGGACTATTGAAGGCTG-3′ (sense for both genotypes), 5′-CGCCTTTTCAGTAGATGGAGG-3′ (antisense for *Nrf2*$^{+/+}$ mice), and 5′-GCGGATTGACCGTAATGGGATAGG-3′ (antisense for LacZ) (36). Mice were fed AIN-76A diet (Harlan Teklad) and had access to water ad libitum; they were housed under controlled conditions (23 ± 2°C; 12-hour light/dark cycles). All experimental protocols conducted on the mice were performed in accordance with the standards established by the US Animal Welfare Acts, as set forth in NIH guidelines and in the Policy and Procedures Manual of the Johns Hopkins University Animal Care and Use Committee.

Exposure to CS. The CS machine for smoke exposure was similar to the one used by Witschi et al. (37). However, the exposure regimen in terms of chamber atmosphere and duration of CS exposure was considerably more intense. At 8 weeks of age, the mice were divided into four groups (n = 40 per group): control *Nrf2* wild-type mice, experimental *Nrf2* wild-type mice, control *Nrf2*-disrupted mice, and experimental *Nrf2*-disrupted mice. The control groups were kept in a filtered air environment, and the experimental groups were subjected to CS for various time periods. CS exposure was carried out (7 hours/day, 7 days/week for up to 6 months) by burning 2R4F reference cigarettes (2.45 mg nicotine per cigarette; purchased from the Tobacco Research Institute, University of Kentucky) using a smoking machine (Model TE-10, Teague Enterprises). Each smoldering cigarette was puffed for 2 seconds, once every minute for a total of 8 puffs, at a flow rate of 1.05 l/min, to provide a standard puff of 35 cm^3. The smoke machine was adjusted to produce a mixture of sidestream smoke (89%) and mainstream smoke (11%) by burning five cigarettes at

one time. Chamber atmosphere was monitored for total suspended particulates and carbon monoxide, with concentrations of 90 mg/m^3 and 350 ppm, respectively.

Morphologic and morphometric analyses. After exposure to CS for various time periods (1.5, 3, and 6 months), the mice (n = 5 per group) were anesthetized with halothane (Halocarbon Laboratories) and the lungs were inflated with 0.5% low-melting agarose at a constant pressure of 25 cm as previously described (38). The inflated lungs were fixed in 10% buffered formalin and embedded in paraffin. Sections (5 μm) were stained with H&E. Mean alveolar diameter, alveolar length, and mean linear intercepts were determined by computer-assisted morphometry with Image Pro Plus software (Media Cybernetics). The lung sections in each group were coded, and representative images (15 per lung section) were acquired with a Nikon E800 microscope (lens magnification, ×20) by an investigator who was blind to the identity of the slides (4).

TUNEL assay. Apoptotic cells in the tissue sections from the agarose-inflated lungs were detected by the Fluorescein-FragEL DNA Fragmentation Detection Kit (Oncogene Research Products) according to the recommendations of the manufacturer. The lung sections (n = 5 per group) were stained with the TdT labeling reaction mixture and mounted with Fluorescein-FragEL mounting medium (Oncogene Research Products). DAPI and fluorescein were visualized at 330–380 nm and 465–495 nm, respectively. Overlapping DAPI in red and FITC in green create a yellow, apoptotic-positive signal. Images (15 per lung section) of the lung sections were acquired with a Nikon E800 microscope (lens magnification, ×20). In each image, the number of DAPI-positive (red) and apoptotic cells (yellow) were counted manually. Apoptotic cells were normalized by the total number of DAPI-positive cells.

Identification of alveolar apoptotic cell populations in the lungs. To identify the different alveolar cell types undergoing apoptosis in the lungs, we performed fluorescent TUNEL labeling in the lung sections from the air- and CS-exposed (6 months) *Nrf2*$^{+/+}$ and *Nrf2*$^{-/-}$ mice, using the Fluorescein-FragEL DNA Fragmentation Detection Kit (Oncogene Research Products). To identify the apoptotic type II epithelial cells in the lungs after TUNEL labeling, we incubated the lung sections first with an anti-mouse SpC antibody and then with an anti-rabbit Texas red antibody. Apoptotic endothelial cells were identified by incubating the fluorescent TUNEL-labeled sections first with the anti-mouse CD34 antibody and then with the biotinylated rabbit anti-mouse secondary antibody. The lung sections were rinsed in PBS and then incubated with the streptavidin-Texas red conjugated complex. The apoptotic macrophages in the lungs were identified by incubating the TUNEL-labeled lung sections first with the rat anti-mouse Mac-3 antibody and then with the anti-rat Texas red antibody. Finally, DAPI was applied to all lung sections, incubated for 5 minutes, washed, and mounted with Vectashield HardSet mounting medium (Vector Laboratories). DAPI and fluorescein were visualized at 330–380 nm and 465–495 nm, respectively. Images of the lung sections were acquired with the Nikon E800 microscope, lens magnification ×40.

Immunohistochemical localization of active caspase-3. Immunohistochemical staining of active caspase-3 was performed using anti-active caspase-3 antibody (39), and the active caspase-3–positive cells were counted with a macro using the Image Pro Plus program (Media Cybernetics) (4). The counts were normalized by the sum of the alveolar profiles, herein named as alveolar length, and expressed in μm or mm. Alveolar length correlates inversely with the mean linear intercept, that is, as the alveolar septa are destroyed, the mean linear intercept increases as total alveolar length decreases.

Caspase-3 activity assay. Caspase-3 activity was assessed using a fluorometric CaspACE Assay commercial kit (Promega Corp.) according to the manufacturer's instructions. Briefly, the frozen lung tissues were immediately homogenized with hypotonic lysis buffer (25 mM HEPES [pH 7.5], 5 mM $MgCl_2$, 5 mM EDTA, 5 mM DTT, 2 mM PMSF, 10 μg/ml pepstatin A, and 10 μg/ml leupeptin) using a mechanical homogenizer on ice and centrifuged at 12,000 *g* for 15 minutes at 4°C. The clear supernatant was collected and frozen in liquid nitrogen. The protein was quantified using Bradford's reagent (Bio-Rad). Lung supernatant containing 30 μg of protein was added to a reaction buffer (98 μl) containing 2 μl DMSO, 10 μl of 100 mM DTT, and 32 μl of caspase assay buffer in a 96-well flat-bottom microtiter plate (Corning-Costar Corp.). The reaction mixture was incubated at 30°C for 30 minutes. Then, 2 μl of 2.5 mM caspase-3 substrate (Ac-DEVD-AMC) was added to the wells and incubated for 60 minutes at 30°C. The fluorescence of the reaction was measured at an excitation wavelength of 360 nm and an emission wavelength of 460 nm. We used 30 μg of protein from anti-Fas antibody–treated Jurkat cells (treated with 1 μg CH11 monoclonal antibody per milliliter of RPMI medium containing 5×10^5 cells for 16 hours at 37°C) as a positive control. A caspase-3–specific inhibitor (2 μl of 2.5 mM DEVD-CHO) was used to show specificity of caspase-3 activity. The activity was below background levels after the addition of caspase-3 inhibitor. These experiments were performed in triplicate and repeated 3 times.

Immunohistochemical localization of 8-oxo-dG. For the immunohistochemical localization and quantification of 8-oxo-dG, lung sections (n = 5 per group) from the mice exposed to CS for 6 months were incubated with anti-8-oxo-dG antibody and stained using the Iso-IHC DAB kit (Inno-Genex) using mouse antibodies. Normal mouse-IgG1 antibody was used as a negative control. The 8-oxo-dG–positive cells were counted with a macro (using Image Pro Plus), and the counts were normalized by alveolar length as described (4).

BAL and phenotyping. Immediately following exposure to CS for 1.5 months or 6 months, mice (n = 8 per group) were anesthetized with sodium pentobarbital. The BAL fluid collected from the lungs of the mice was centrifuged (500 *g* at 4°C), and the cell pellet was resuspended in PBS. The total number of cells in the lavage fluid was determined, and 2×10^4 cells were cytocentrifuged (Shandon Southern Products) onto glass slides and stained with Wright-Giemsa stain (Diff-Quik; Baxter Scientific Products). Differential cell counts were performed on 300 cells, according to standard cytologic techniques (40).

Immunohistochemical localization of inflammatory cells in the lungs. Macrophages were identified by the rat anti-mouse Mac-3 and secondary biotinylated anti-rat antibody immunostaining using the Vector RTU HRP-avidin complex with 3,3′-diaminobenzidine as the chromogenic substrate. The number of Mac-3–positive cells in the lung sections (n = 3 per group and 10 fields per lung section) were counted manually and normalized by alveolar length.

EMSA. EMSA was carried out according to a procedure described previously (41). For gel shift analysis, 10 μg of nuclear protein that had been prepared from the lungs of mice exposed to air or to CS for 5 hours was incubated with the labeled human NQO1 ARE, and the mixtures were analyzed on a 5% nondenaturing polyacrylamide gel. To determine the specificity of protein(s) binding to the ARE sequence, 50-fold excess of unlabeled competitor oligo (ARE consensus sequence) was incubated with the nuclear extract for 10 minutes prior to the addition of radiolabeled probe. For supershift analysis, the labeled NQO1 ARE was first incubated for 30 min with 10 μg of nuclear proteins and then with 4 μg of anti-Nrf2 antibody for 2 hours. Normal rabbit IgG_1 (4 μg) was used as a control for the supershift assay. The mixtures were separated on native polyacrylamide gel and developed by autoradiography. The P^{32}-labeled consensus sequence for OCT1 was used as a control for gel loading. The EMSA was performed 3 times with the nuclear proteins isolated from 3 different air- or CS-exposed *Nrf2*$^{+/+}$ and *Nrf2*$^{-/-}$ mice.

Western blot analysis. Western blot analysis was performed according to previously published procedures (41). To determine the nuclear accumu-

lation of Nrf2, we used 10% SDS-PAGE to separate 50 μg of the nuclear proteins isolated from the lungs of air- or CS-exposed (5 hours) *Nrf2*$^{+/+}$ and *Nrf2*$^{-/-}$ mice. Then, we electrophoretically transferred them onto a PVDF membrane (Millipore). The membranes were blocked with 5% (w/v) BSA in Tris-buffered saline (20 mM Tris/HCl [pH 7.6] and 150 mM NaCl) with 0.1% [v/v] Tween-20 for 2 hours at room temperature, and then incubated overnight at 4°C with polyclonal rabbit anti-Nrf2 antibody, followed by incubation with HRP-conjugated secondary antibody. The blots were developed using an enhanced chemiluminescence Western blotting detection kit (Amersham Biosciences). Then, the blots were stripped and reprobed with anti-lamin B1 antibody.

To identify the active caspase-3, the lung tissues ($n = 3$) were homogenized with the lysis buffer (containing 50 mM Tris/HCl [pH 8.0], 150 mM NaCl, 0.5% (v/v) Nonidet P40, 2 mM EDTA, and a protease inhibitor cocktail) on ice using a mechanical homogenizer. Following centrifugation at 12,000 *g* for 15 minutes, the protein concentration of the supernatant was determined using Bradford's reagent. Equal amounts of protein (30 μg) were resolved on 15% SDS-PAGE and transferred onto a PVDF membrane (Millipore). The membranes were incubated with rabbit anti-caspase-3 antibody and then with secondary anti-rabbit antibody linked to HRP conjugate. The blots were developed using the enhanced chemiluminescence Western blotting detection kit (Amersham Biosciences). Thereafter, blots were stripped and reprobed with antibodies to actin. Western blot was performed thrice with protein extracts from 3 different air- or CS- exposed (6 months) *Nrf2*$^{+/+}$ and *Nrf2*$^{-/-}$ mice. Band intensities of procaspase-3 and active caspase-3 of the 3 blots were determined using NIH Image-Pro Plus software. Values are represented as mean ± SEM.

Transcriptional profiling using oligonucleotide microarrays. Lungs were excised from control (air-exposed) and CS-exposed (5 hours) mice ($n = 3$ per group) and processed for total RNA extraction using the TRIzol reagent (Invitrogen). The isolated RNA was used for gene expression profiling with Murine Genome U74A version 2 arrays (Affymetrix) using procedures described earlier (42). To identify the differentially expressed transcripts, pairwise comparison analyses were carried out with the Data Mining Tool 3.0 program (Affymetrix). Only those differentially expressed genes that appeared in at least 6 of the 9 comparisons and showed a change of more than 1.4-fold were selected. In addition, the Mann-Whitney pairwise comparison test was performed to rank the results by concordance as an indication of the significance ($P \leq 0.05$) of each identified change in gene expression. Genes which were upregulated only in the lungs of wild-type mice in response to CS were selected and used for the identification of AREs in their upstream sequence.

Identification of AREs in Nrf2-regulated genes. To identify the presence and location of AREs in Nrf2-dependent genes, the murine homologs of human genes were employed (Human Genome *build 34*, version 1, the National Center for Biotechnology Information [NCBI] database). For every gene, a 10-kb sequence upstream from the transcription start site (TSS) was used to search for AREs with the help of Genamics Expression 1.1 Pattern Finder Tool software (Genamics) using the primary core sequence of ARE (RTGAYNNNGCR) (43) as the probe. TSS for all the genes was determined by following the Human Genome *build 34*, version 1, of the NCBI database.

Northern blotting. Northern blotting was performed according to the procedure described earlier (42). In brief, 10 μg of total RNA isolated from the lungs of air- and CS-exposed (5 hours) mice ($n = 3$) was separated on 1.2% agarose gel, transferred to nylon membranes (NYTRAN Super Charge; Schleicher & Schuell), and ultraviolet-crosslinked. Full-length probes for NQO1, γ-GCS (regulatory subunit), GST-α1, HO-1, TrxR, Prx-1, GSR, G6PDH, and β-actin were generated by PCR from the cDNA of murine liver. These PCR products were radiolabeled with [α-^{32}P] cytidine triphosphate (CTP) and hybridized using QuickHyb solution (Stratagene) according to the manufacturer's protocol. After the films were exposed to the phosphoimager screen for 24 hours, hybridization signals were detected using a Bioimaging system (BAS1000, Fuji Photo Film). Quantification of mRNA was performed using Scion image analysis software (Scion Corporation). Levels of RNA were quantified and normalized for RNA loading by stripping and reprobing the blots with a probe for β-actin.

Enzyme activity assays. For measuring enzyme activity of selected genes, mice were exposed to CS for 5 hours and sacrificed after 24 hours. The lungs were excised ($n = 3$ per group) and processed as described (21) to measure the activities of NQO1, G6PDH, GPx, Prx, and GSR. GPx activity was measured according to the procedure of Flohe and Gunzler (44). NQO1 activity was determined using menadione as a substrate (45). The peroxidase activity of Prx was measured by monitoring the oxidation of NADPH as described (46). G6PDH activity was determined from the rate of glucose 6-phosphate-dependent reduction of $NADP^+$ (47). GSR activity was determined from the rate of oxidation of NADPH by using oxidized glutathione as substrate (48). Protein concentration was determined by using the Biorad reagent, with bovine serum albumin as the standard. The values for enzyme-specific activities are given as means ± SE. Student's *t* test was used to determine statistical significance.

Statistical analysis. Statistical analysis was performed by ANOVA, with the selection of the most conservative pairwise multiple comparison method using the program SigmaPlot 2000 (SPSS Inc.), and differences between groups were determined by Student's *t* test using the InStat program (GraphPad Software Inc.).

Acknowledgments

This work was supported by National Institute of Environmental Health Sciences Center grant P30 ES 03819; the Maryland Cigarette Restitution Fund (to S. Biswal); the Flight Attendant Research Institute (to S. Biswal); Alpha – 1 Foundation (to R.M. Tuder and I. Petrache); the American Thoracic Society and the American Lung Association (to I. Petrache); and NIH grants P50 CA058184, R01 66554 (to R.M. Tuder), and R01 CA94076 (to T.W. Kensler). We thank Wayne Mitzner for the total lung capacity measurements.

Received for publication January 23, 2004, and accepted in revised form September 7, 2004.

Address correspondence to: Shyam Biswal, Division of Toxicological Sciences, Department of Environmental Health Sciences, Bloomberg School of Public Health, Johns Hopkins University, Baltimore, Maryland 21205, USA. Phone: (410) 955-4728; Fax: (410) 955-0116; E-mail: sbiswal@jhsph.edu.

Chung Y. Cho and Rajesh K. Thimmulappa contributed equally to this work.

1. Mahadeva, R., and Shapiro, S.D. 2002. Chronic obstructive pulmonary disease * 3: Experimental animal models of pulmonary emphysema. *Thorax.* 57:908–914.
2. Petty, T.L. 2003. Definition, epidemiology, course, and prognosis of COPD. *Clin. Cornerstone.* 5:1–10.
3. Viegi, G., Scognamiglio, A., Baldacci, S., Pistelli, F., and Carrozzi, L. 2001. Epidemiology of chronic obstructive pulmonary disease (COPD). *Respiration.* 68:4–19.
4. Tuder, R.M., et al. 2003. Oxidative stress and apoptosis interact and cause emphysema due to vascular endothelial growth factor receptor blockade. *Am. J. Respir. Cell Mol. Biol.* 29:88–97.
5. Eriksson, S. 1964. Pulmonary emphysema and α1-antitrypsin deficiency. *Acta Med. Scand.* 175:197–205.
6. Joos, L., Pare, P.D., and Sandford, A.J. 2002. Genetic risk factors of chronic obstructive pulmonary disease. *Swiss Med. Wkly.* 132:27–37.
7. Hautamaki, R.D., Kobayashi, D.K., Senior, R.M.,